Akademie věd České republiky

Teze disertace
k získání vědeckého titulu "doktor věd"
ve skupině věd chemických věd

Chemical Engineering Aspects of Gas Transport in Porous Solids

Komise pro obhajoby doktorských disertací v oboru Chemické inženýrství

Jméno uchazeče: Olga Šolcová

Pracoviště uchazeče: Ústav chemických procesů, AV ČR, v.v.i.

Místo a datum 17. 10. 2011

1 Introduction

The industrial application of porous solids is quite widespread. Porous heterogeneous catalysts, adsorbents and membranes are used in chemical industry and in biotechnology, porous materials are common in building engineering, porous catalysts form the basis of mufflers in cars, etc. The rates of processes which take place in the pore structure of these materials are affected or determined by the transport resistance of the pore structure. Inclusion of transport processes into description of the whole process is essential when reliable simulations/predictions have to be made. Trends, in modern chemical/biochemical reaction engineering, point to utilisation of more sophisticated and therefore more reliable models of processes. The basic idea is that the better the description of individual steps of the whole process the better its description and, perhaps, even extrapolation. Dependable process description forms the basis of process control and process optimisation. For example optimum pore structure of adsorbents, membranes, enzyme/cell supports or heterogeneous catalysts can be suggested which will guarantee best activity or selectivity. Similarly, optimum operation conditions can be found when the process description is based on as full as possible knowledge of process steps.

Because of the unique nature of pore structure of various materials, the pore structure characteristics relevant to transport in pores have to be determined experimentally. Two approaches have been used in this respect: i) textural analysis of the porous solid, ii) evaluation of simple transport processes taking place in the porous solid in question. The advantage of the first approach derives from the complexity of available experimental methods and evaluation procedures (physical adsorption of gases, high-pressure mercury porosimetry, liquid expulsion permporometry, permporometry with pores blocked by capillary condensation, etc.). The relevance of the second approach stems from the possibility to use the same pore-structure model as used in description of the process in question (counter-current (isobaric) diffusion of simple gases, permeation of simple gases under steady-state or dynamic conditions, combined diffusion and permeation of gases under dynamic conditions, etc.).

The aim of this study is summarization of knowledge of the experimental methods suitable for material characteristics relevant to the gas transport in porous solids with respect to the chemical engineering aspects. Evaluation of various unique methods is described including their mutual correlations in connection with their practical use. The chromatographic method with special evaluation system based on the developed interpolation equations that enables determination of the effective diffusion coefficients as well as transport

parameters for any shape of porous materials is also introduce. Finally the applications of individual methods for practical use are shown.

The thesis summarized research concerning the experimental methods suitable for obtaining material characteristics relevant to chemical engineering aspects of the gas transport in porous solids that was done since 1991. The thesis is based on my 30 articles and chapters in books (indicated O (own) and number) and five doctoral theses (two defended, three before defense; all supervised by author). Research summarized in the Thesis was supported by twelve projects in which I acted as the principal scientist from various grant agencies (EU, GA CR, GA AV, AV CR, TA CR, MIT).

2 Texture of porous solids

The topic of the chapter has been solved in the scope of projects A4072915 (Complex Textural Characterization of Porous Solids Regarding the Mutual Relationship of Different Methods), GA104/04/0963 (Nanostructured Materials – Texture from Physical Adsorption), KAN400720701 (Hierarchic Nanosystems for Microelectronics) and GA104/09/0694 (Advanced Photocatalytic Processes- Nanotechnology for Environment) and is based on results summarized in articles O26, O37, O38, O44, O45, O49, O66 and doctoral thesis (L. Matějová, Nanostructure materials, texture from physical adsorption, 2008).

Knowledge of porous material texture belongs to basic information inevitable for their applications. Nowadays, there are a number of chemical or physical methods that have been used for the pore structure characterization as SAXS, XRD, TEM, SEM, FTIR, NMR studies etc. Nevertheless, two methods are applied routinely for the analysis of texture of porous solids; physical adsorption of inert gases (e.g. nitrogen, argon, krypton) and high-pressure mercury porosimetry. Both methods are nearly exclusively performed on the automatic commercial instruments that differ mainly in the highest operative pressure (for mercury porosimetry measurement) or in the lowest relative pressure used for evaluation of physisorption isotherms.

2.1 Classic texture methods

Recent years are characterized by a huge progress in preparation of novel materials [1-4]. These materials possess unique structure (ordered or disordered mesoporous structure with and/or without micropores – see Fig 1 for the better imagination), which significantly influences their properties [5-9]. Therefore, the detailed information on material texture (pore-size distribution (PSD), specific surface area (BET), micropore volume, surface area of mesopores etc) is inevitable for their possible application. Thus a great attention has been paid to improvement of data evaluation.

A number of models can be used for obtaining PSD's for cylindrical pore geometry from physical adsorption data; different dependences for

adsorbed thickness as well as diverse evaluation algorithms can be applied [10-22]. All models simplify the real structure of any new materials rather drastically, which can produce significant differences in evaluated textural properties and may cause problems in further utilization of these materials. [O38]

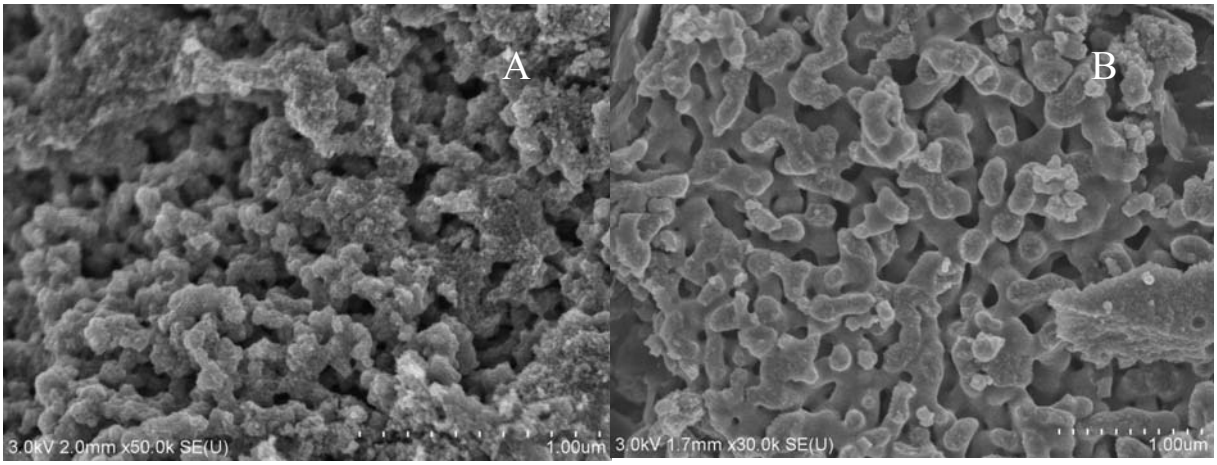

Fig. 1 Two titania powders prepared by various routes with the significantly different amount of micropores [O49].

The other complication is the presence of micropores that makes the textural analysis based on transformation of adsorption isotherms much less straightforward than in the case of porous solids with mesopores only. The simple BET analysis [24] is, nevertheless, usually (and incorrectly) performed. The reason is that the simple BET isotherm was developed explicitly for non-microporous (i.e. mesoporous) solids and in the relative pressure range, x_{BET}, which guarantees no capillary condensation in pores (e.g. $0.25 > x_{BET} > 0.05$). The correct way is to use the comparative plots (t-plots, α-plots) which can supply the micropore volume, a_μ, as well as the mesopore surface area, S_m, or the three-parameter BET [25, O45].

The other possibility is the application of experimentally determined standard (master) isotherms, which show the physical adsorption of an inert gas on a nonporous sample of the same/similar chemical composition as the porous sample being analyzed [O44]. In textural analysis the standard (master) isotherms appear in two places; for the construction of pore-size distributions (PSD's) from physical adsorption data and for determination of volume of micropores and area of mesopores by t-plot or α–plot methods.

It can be summarized that regardless of a huge progress in the texture properties evaluation situation seems to be rather more complicated. From that reasons the advantages and disadvantages of various models commonly used for obtaining PSD's from physical adsorption data were compared for sixteen combinations of models and evaluation algorithms including the Nonlinear

Density Functional Theory (NLDFT). The significant differences in evaluated textural properties by individual models were found between several to more then thirty percent (with the worth results evaluated by the NLDFT method). The failure of the classic BET analysis for microporous-mesoporous samples was also shown together with the correct approach to the texture evaluation of samples which include micropores. To enable the evaluation of more precise texture properties of the significant types of materials the experimentally determined standard (master) isotherms (inaccessible in literature) were measured, evaluated and published [O44] for nitrogen as well as for argon. Simultaneously, it was determined that comparison of results from nitrogen adsorption at 77 K and argon adsorption at 87 K is rather limited.

Despite of this effort the information on material texture must be correlated and applied with respect to data acquisition. It is also necessary to consider if information on texture properties evaluated by classic texture analysis that perform analyses over the sufficient amount of sample (usually 0.2 – 1 g), but take into account all pores (blind as well through pores) are suitable as the material description for the process optimization. Both mentioned texture methods are frequently used, but they are far from being the best choice; intrusion of a liquid metal into pores or multilayer physical adsorption and condensation e.g. of nitrogen at 77 K are governed by completely different laws than gas transport.

2.2 Liquid expulsion permporometry

There are existed methods, the *permporometry* methods, which enable determination of the pore-size distribution of the flow-through pores in a porous medium which is significant for a majority of processes/applications. Perporometry methods gained a fresh impetus with the advance of porous membranes. They have been frequently used for structural characterization of membranes [29,30]. It allows detection of nano-size membrane pores [31] and checking the quality of synthesized membranes [32]. Similarly, the effect of filter filler particle size distribution can be established [33,34]. Generally, materials routinely tested by permporometry (membranes, filters, fibers, textiles, etc.) have one common feature – a very low thickness, always under one millimeter and usually about tens or hundreds of microns. The basic idea of this method is to block pores of some sizes by a wettable liquid and measure either permeation or diffusion through the open pores.

In the liquid-expulsion permporometry, LEPP, [O26], the porous solid is saturated with a liquid and by application of a pressure difference across the sample the liquid is forced out of the largest pores. The rate of gas permeating through these pores is then measured. Then, the pressure difference is increased which frees another pores, etc. As a result, pore-size distribution is obtained.

Nevertheless, for evaluation of the pore-size distribution of flow-through pores for pelleted porous catalysts, adsorbents and similar solids with larger thicknesses (about 5 mm) the more realistic description of the gas permeation process was necessary to suggest. Not only pellet thickness is far larger, but also pores are much narrower than in porous membranes, filters, fibers or textiles. Thus Knudsen transport (significant for narrow pores) must be takes into account besides viscous transport (significant for larger pores) In articles [O26, O37] the newly design, constructed and tested experimental laboratory set-up is applied for verification of two evaluated measurement modes based on Darcy's constitutive equation with permeability coefficient given by the Weber equation.

For better imagination in Fig 2 the pore-size distribution curves obtained from mercury porosimetry are compared with distribution curves obtained by LEPP method for three various samples. PSD's from LEPP are narrower than from mercury porosimetry and shifted to smaller pores. This is caused by blind pores that are only detected by mercury porosimetry.

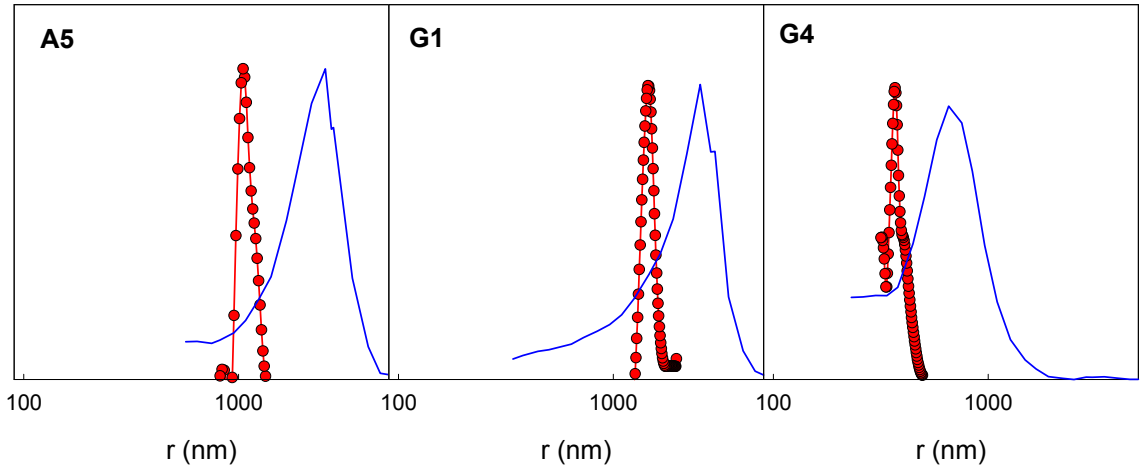

Fig. 2 Comparison of the pore-size distribution curves obtained from mercury porosimetry (blue line) with distribution curves obtained by LEPP method (red line with experimental points) [O26]

It can be summarized that in our laboratory the new permporometry method that enables evaluation of the pore-size distribution of the flow-through pores was developed. The special laboratory apparatus was designed and constructed. Applicability of this method was tested on various types of porous materials and verified for the wide range of pore-sizes (10 nm - 20 μm).

3 Transport parameter evaluation

The subject of this chapter has been solved in the scope of projects A4072915 (Complex Textural Characterization of Porous Solids Regarding the Mutual Relationship of Different Methods), A4072706 (Permeation of Gases in Porous Solids), P1-010-601 (Physical and Chemical Properties of Surfaces and Catalysis), P204/11/1206 (Use of PFG NMR, stochastic reconstruction and molecular simulation to estimate transport-related texture characteristics of advanced porous materials) and it is based on results summarized in articles O9, O12, O16, O19, O24, O25, O46, O47, O75 and doctoral thesis (K. Soukup, Multiphase diffusion in pores and validity of Graham law, 2006).

Any prediction or simulation of gas transport in porous solids is based on mass balances. The balance equations incorporate inevitable constitutive equations, which relate the intensity of mass flux to mass flux driving forces. Constitutive equations comprise information of three kinds [O75]:

1) Properties of components of the gas mixture: bulk diffusion coefficients of all pairs of components of the gas mixture, component viscosities and their mean speeds. Such properties are, usually, readily available.

2) The physical laws, which describe the gas transport, with idealized units of the porous medium. Usually, cylindrical capillaries are utilized because of the availability and simplicity of the laws.

3) Characteristics of the porous medium. Since the diverse complicated nature of the porous medium is usually unknown it must be modeled. Modeling of the porous structure is based on idealized geometrical units for which the description of gas transport follows from physical laws and thus the evaluated texture properties do not correspond to the real pore networks. Fig. 3 illustrates the variability of the porous structure of some porous materials.

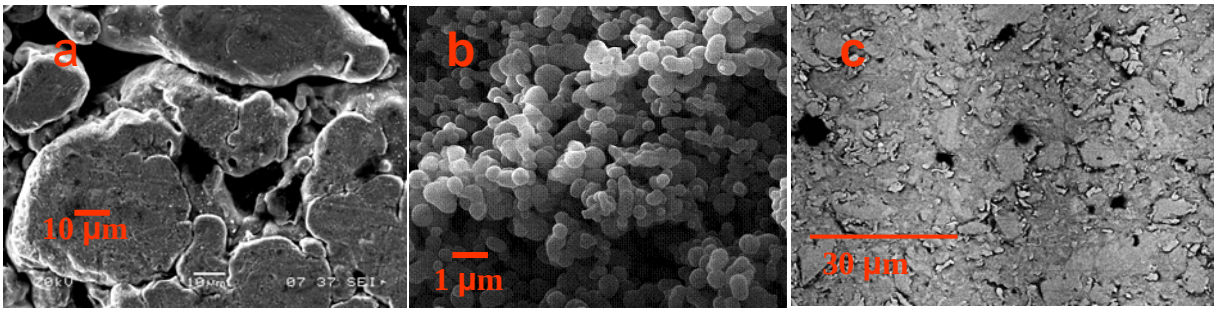

Fig. 3 variability of the porous structure, a – iron pellets produce by powder metallurgy, b –silica SBA-15, c – catalyst SA-6873, Norton, England

There are existed only few models which describe combined (diffusion and permeation) transport of multicomponent gas mixtures through the porous medium [35-37], nevertheless only two models seem to be the most relevant

and usually used for description of combined transport of multicomponent gas mixtures: the Mean Transport-Pore Model (MTPM) [38,39] and the Dusty Gas Model (DGM) [40,41].

Mean Transport-Pore Model (MTPM) assumes that the decisive part of the gas transport takes place in transport-pores that are visualized as cylindrical capillaries with radii distributed around the integral mean value <r> (first model parameter). The width of this distribution is characterized by the integral mean value of the squared transport-pore radii, $< r^2>$ (second model parameter). The third model parameter is the ratio of porosity, ε_t, and tortuosity of transport-pores, q_t, $\psi = \varepsilon_t/q_t$ [34,42].

Dusty Gas Model (DGM) visualizes the porous medium as a collection of giant spherical molecules (dust particles) kept in space by external force. The movement of gas molecules in the spaces between dust particles is described by the kinetic theory of gases. Formally, two of MTPM transport parameters, <r> and $< r^2>$, can be used also in DGM. The third MTPM parameter, ψ, characterizes the effective porosity of transport-pores, ε_t, and accounts also for their tortuosity, q_t ($\psi \equiv \varepsilon_t/q_t$). The third DGM transport parameter, B_0, characterizes the viscous (Poiseuille) gas flow in pores and can be, formally, replaced by $<r^2>\psi/8$.

3.1 Constitutive equation

The net molar flux density of component i in a n-component gas mixture per unit *total* cross-section of the porous solid, N_i, due to the combined influence of composition gradients and total pressure gradient in a porous solids is given as the sum of the permeation molar flux density of component i, N_i^p, and the diffusion molar flux density of this component, N_i^d, [43]:

$$N_i = N_i^p + N_i^d \qquad i=1,..., n \tag{1}$$

For the net mixture molar flux density, N, it follows

$$N = N^p + N^d \qquad i=1,..., n \tag{2}$$

where N^d is the mixture net molar diffusion flux density ($N^d = \sum_{i=1}^{n} N_i^d$) and N^p is the mixture net molar permeation flux density ($N^p = \sum_{i=1}^{n} N_i^p$).

In MTPM and DGM the steady-state isothermal diffusion transport in multicomponent gas mixtures, for cylindrical pores with diameter <r> and the transition region (i.e. when the pore diameter, 2 <r>, is comparable with the mean free-path length of gas molecules, λ; $2<r> \approx \lambda$), is described by the modified Maxwell-Stefan equation [44]:

$$\frac{N_i^d}{D_i^k} + \sum_{\substack{j=1 \\ j\neq i}}^{n} \frac{y_j N_i^d - y_i N_j^d}{D_{ij}^m} = (df)_i \qquad i=1,..., n \tag{3}$$

(df) is the driving force, y_i the mole fraction of component i, D_{ij}^m is the effective diffusion coefficient of the pair i-j in the bulk diffusion region:

$$D_{ij}^m = \psi \mathcal{D}_{ij}^m \tag{4}$$

and D_i^k ,is the effective Knudsen diffusion coefficient of component i:

$$D_i^k = \psi \langle r \rangle K_i \tag{5}$$

with the Knudsen coefficient K_i

$$K_i = \frac{2}{3}\sqrt{\frac{8R_gT}{\pi M_i}} \tag{6}$$

The driving force term $(df)_i$ differs for MTPM and DGM:

MTPM $$(df)_i = -c_T \frac{dy_i}{dx} \tag{7}$$

DGM $$(df)_i = -\frac{d(c_T y_i)}{dxi} \tag{8}$$

c_T is the total molar concentration of the gas mixture and x is the length coordinate in the transport direction. For pure (isobaric) diffusion, where $dc_T/dx=0$, both driving forces (7), (8) are identical: $-d(c_T y_i)/dx = -c_T dy_i/dx$. The (rather small) difference starts to appear in combined diffusion and permeation cases.

By summing modified Maxwell-Stefan isobaric diffusion equations (3) for all gas mixture components the generalized Graham's law appears

$$\sum_{i=1}^{n} N_i^d \sqrt{M_i} = 0 \tag{9}$$

which is the condition that must be fulfilled in order to have pure diffusion mass transport.

The MTPM permeation molar flux density of gas mixture component i, $N^p{}_i$, in porous solids is described by the Darcy equation:

$$N_i^p = -y_i B_i \frac{dc_T}{dx} \qquad i=1,..., n \tag{10}$$

B_i is the effective permeability coefficient of mixture component i [34]:

$$B_i = < r > \psi K_i \frac{\omega \nu_i + Kn_i}{1 + Kn_i} + \frac{\langle r^2 \rangle \psi p}{8\eta} \quad i=1,.., n \tag{11}$$

which includes the MTPM transport parameters, ψ, $<r>$, $< r^2>$. The numerical coefficient ω depends on the details of the wall-slip description (ω = 0,9, $\pi/4$, $3\pi/16$, etc.; see [34]); ν_i is the square root of the relative molecular weight of the gas mixture component i:

$$\nu_i = \sqrt{M_i / \sum_{j=1}^{nj} y_j M_j} \tag{12}$$

η is the gas mixture viscosity and Kn_i is the Knudsen number of component i ($Kn_i \equiv \lambda_i / 2\langle r \rangle$) based on mean free-path length of component i in the gas mixture.

The DGM permeation molar flux density of component i, N_i^p, is described by Darcy law

$$N_i^p = -y_i B \frac{dc_T}{dx} \qquad i=1,..., n \tag{13}$$

with identical effective permeability coefficients, B, for all gas mixture components:

$$B = B_o p / \eta \qquad i=1,..., n \tag{14}$$

B_O is the third DGM transport parameter that can be, formally, replaced by $\langle r^2 \rangle \psi / 8$.

3.2 Transport parameters

The unknown real pore structure makes an *a priori* determination of transport characteristics unfeasible. The pore structure characteristics relevant to transport in pores have to be determined experimentally. Two approaches can be used in this respect: (i) textural analysis of the porous solid and (ii) evaluation of simple transport processes taking place in the porous solid in question.

The advantage of textural analysis of the porous solid derives from the wealth of available experimental methods and evaluation procedures (physical adsorption of gases, high-pressure mercury porosimetry, etc.). These methods are frequently used, but they are far from being the best choice (as was shown in Chapter 2.1), for as much as that used methods are governed by completely different laws than gas transport. [38].

The relevance of evaluation of transport parameters from simple transport processes which take place in the porous solid in question stems from the possibility to use the same pore-structure model both for evaluation of transport parameters and for description of the process in question. It is a good idea to use a mass transfer process, which is similar to the gas transport process under consideration. It is of advantage to choose for determination of transport parameters a (simple) process that can be easily followed at near-laboratory conditions and does not require sophisticated instrumentation.
Various choices can be made:

- pure counter-current diffusion of gas mixtures under steady-state conditions;
- binary diffusion under dynamic conditions;
- dynamic or steady-state permeation of individual gases;
- combined diffusion and permeation gas transport.

At the same time it is a good choice to use inert (i.e. nonadsorbable) gases; this eliminates transport of adsorbed gas along the surface of pores (surface diffusion) the nature of which is not very well understood.

The best way for experimental evaluation of transport parameters (material constants that are independent on pressure, temperature as well as the composition of used gases) are the following simple transport processes. At least four combinations of transport processes can be used.

3.3 Steady-state counter-current diffusion

Binary and multicomponent counter-current diffusion of pure gases has been the standard way for studying isobaric diffusion in porous solids [O19]. Wicke and Kallenbach [45] developed their classic cell for steady-state measurements of this type and since that time diffusion has been frequently studied. To determinate transport characteristics (transport parameters) of porous solids Dogu and Smith [46] developed the dynamic version of the Wicke-Kallenbach diffusion cell; for data evaluation the moment method was applied. The effect of combined steady-state diffusion- and convection transport in a porous medium on the catalytic reaction rate was studied by Haynes [47]. Krishna [48,49] focused on a similar problem. Results on dynamics of combined diffusive and viscous transport in capillaries for multicomponent gas mixtures were reported by Do and Do [50]. Krishna and Wesselingh [51] reviewed the Maxwell-Stefan approach to mass transfer. Diffusion in zeolites and porous membranes is another rapidly growing area of application of Stefan-Maxwell approach (e.g. [52-54].

3.3.1 Wicke-Kallenbach diffusion cell

The classic Wicke-Kallenbach cell consists of upper and lower compartment and a metallic disc with cylindrical holes sandwiched between both compartments. A porous pellet is forced into undersized rubber tubing and the pellet-tubing assemblies are then forced into holes of the metallic disc. The absence of gaps between porous pellets and rubber tubes as well as between rubber tubes and metallic surfaces of disc holes can be verified by replacing porous pellets by identically sized metallic cylinders. One gas flows steadily through one cell compartment and another gas through the other cell compartment; both chambers are kept at the constant temperature and at the precisely same pressure. The outlet gas streams from both compartments are analyzed for the content of the gas from the opposing compartment (mole fractions y_B^U, y_A^L). Gases in both cell compartments should be ideally mixed, i.e. composition in the compartment have to be the same as at the compartment outlets.

Fig. 4 Detail of the Wicke-Kallenbach cell [O46]

The main disadvantage of the classic Wicke – Kallenbach cell (see Fig. 4) besides the necessity to monitor composition of the two outlet gas streams is the strict requirement of equal pressure in both cell compartments (even small pressure differences between compartments can cause large errors due to the intrusion of the viscous flow).

3.3.2 Graham diffusion cell

The two-component version of the general Graham's law (Eq. (9)) reads

$$\frac{N_A^d}{N_B^d} = -\sqrt{\frac{M_B}{M_A}} \tag{15}$$

where M_A and M_B are molecular weights of A and B. Thus, in binary countercurrent diffusion the diffusion fluxes are not equimolar as is often assumed. The minus sign in Eq.(15) reflects the opposite directions of the molar diffusion flux densities. For gases with different molecular weight this ratio is far from unity. Thus, the net diffusion flux, $N^d = N^d_A + N^d_B$, is nonzero. This offers a simple way for determination of flux densities of individual gases simply by following the net diffusion flux, N^d.

Thus, it is not necessary to monitor the composition of both gas streams at the outlets of cell compartments and the main disadvantage of the Wicke-Kallenbach cell (viz. equality of pressure in both compartments) is removed because both compartments are open to atmosphere and, hence, no special pressure regulation is required. Disadvantage of this cell stems from the fact, that the more different the molecular weights of both gases the higher the net molar diffusion flux density, N^d, and the more accurate is its determination. However, gases with high molecular weights tend to adsorb, which can cause (unwanted) surface diffusion to occur. This restricts the choice of suitable gas pairs to nonadsorbable inerts (e.g. H_2, He, N_2, Ar). The volume of experimental information can be increased by replacing one of the gases (say A) by a binary mixture with gas B (gas system (A+B) vers. B) or with another gas C (gas system (A+C) vers. B) in order to increase the confidence of evaluated transport parameters. In Fig 11 the excellent agreement of

experimental and calculated net volumetric diffusion flux densities is easily seen. Equations corresponding to the use of more than two gases can be found elsewhere [O19].

If net diffusion flux densities, N^d, are experimentally determined for different gas pairs A – B, then it is possible to obtain the corresponding transport parameters <r> and ψ [O25]. Fig. 5 shows 95% confidence regions of transport parameters for several commercial and laboratory-prepared porous catalyst pellets evaluated from an equivalent for three-component gas systems ((A+B) vers. B and (A+C) vers. B). The optimum parameter sets are marked as circles. It is interesting that the shape of the confidence region is intimately connected with the region in which the diffusion process takes place. There are two limiting diffusion mechanisms: the Knudsen diffusion, which appears only in narrow pores and the bulk diffusion mechanisms, which takes place in wide pores. In the transition diffusion region both mechanisms play a role and the contribution of each mechanism can be seen from the shape of the confidence region.

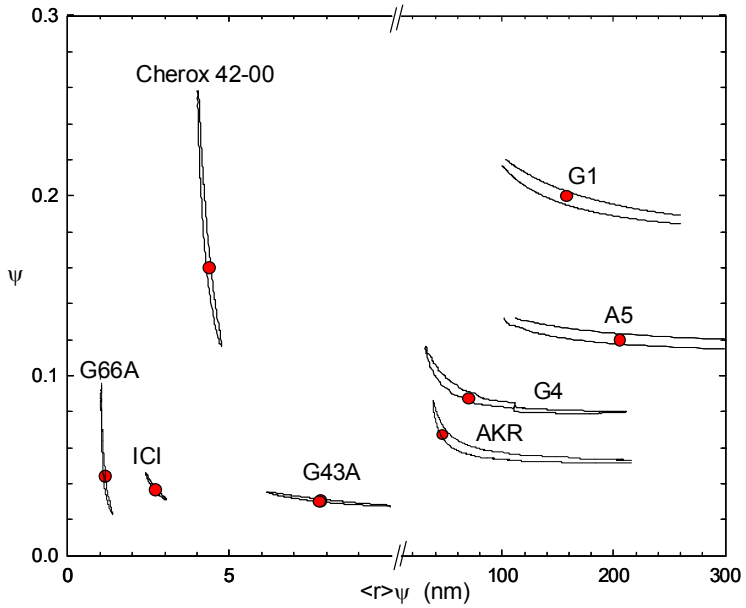

Fig. 5 95% confidence regions of transport parameters for porous pellets with various pore-size distributions; red points – the evaluated transport parameters [O25]

Comparison of the Wicke-Kallenbach and Graham diffusion cells for transport characteristics of porous solid determination is shown in next study [O46] on a series of porous samples with a broad range of pore radii (from 78 nm up to 10 μm). Differences between diffusion fluxes from both diffusion cells were always bellow 5 % and did not exceed the experimental error in the

whole range of tested pore radii. Also the experimental and calculated diffusion fluxes agreed perfectly, but only for porous materials with pore radii smaller than several micrometers. For materials with larger pore radii (above 7 μm) significant deviations appear due to intruding permeation transport caused by the very small pressure difference between compartments of the Wicke-Kallenbach as well as Graham's diffusion cells. These tiny pressure differences (about several Pascals) are unavoidably present even under cautious experimental conditions [O47] and become significant for samples with pore radii above 7 μm. Moreover the error caused by permeation flux significantly rises with the pore radius increase; for 7 μm the error is about 5% and for 21 μm is about 50%! The only possibility is the independent determination of permeation characteristics and consequent "purification" of diffusion fluxes. Without that the diffusion fluxes can not be used for further calculations of, e.g. effective diffusion coefficients inevitable for chemical engineering calculations, process development and design.

It is necessary to stress that in the Wicke –Kallenbach and Graham diffusion cell binary and multicomponent counter-current diffusion of pure gases can be studied. Both cells allow determination of the net diffusion flux densities through the pelleted porous solids and, thus, to obtain the corresponding transport parameters $\langle r \rangle$ and $\langle r \rangle \psi$. Connection of these parameters to the region, in which the diffusion process takes predominately place, was shown in article O25. In the mentioned article there is also noticeable that the contribution of each mechanism can be evaluated from the shape of the 95% confidence regions of transport parameters. Verification of the Graham's law together with the applicability of evaluated effective diffusion coefficients (in Wicke-Kallenbach as well as Graham's diffusion cells) for materials with the wide range of porous structure were published in articles O46 and O47. Material structure and all transports through the porous medium must be taken into account before chemical engineering calculations, process development as well as design.

3.4 Pseudo-stationary and dynamic permeation

Transport parameters $\langle r \rangle \psi$ and $\langle r^2 \rangle \psi$ can be evaluated from permeation measurements (single gas flow-rate under controlled pressure gradient) performed with pure gases [O75]. The corresponding permeation cells can be designed for measurements under steady state as well under dynamic conditions. To gather sufficient experimental information measurements must be repeated for different pressures and different gases. The steady-state permeation requires control of pressures and determination of flow-rates at these pressures. The last task is by no means simple. It is therefore reasonable to use pseudo-stationary or dynamic permeation cells.

Both the pseudo-stationary and dynamic cells consist of upper and lower compartments and a metallic disc with cylindrical holes filled by pellets

of porous solid, similar as in the Wicke-Kallenbach and Graham diffusion cells. The cells differ mainly in compartment volumes, inlet and outlet gas lines (with valves) and the attached pressure- /differential pressure-transducers. The number of pellets in the metallic disc and the volumes of cell compartments affect the permeation rate. Thus, their change can be used for obtaining pressure responses compatible with capabilities of the used pressure transducer. [O24].

3.4.1 Pseudo-stationary cell

Identical compartment volumes $V = V_L = V_U$ are the basic precondition. After evacuation both compartments are filled with permeation gas up to initial pressure P^o. At run start the gas pressure in the upper cell compartment is increased by a small amount (usually 500-900 Pa), ΔP^o, and the gas inlet is closed. The time-change of the pressure difference between compartments, $\Delta P(t)$, is followed by the differential pressure transducer.

The exponential decay of $\Delta P(t)$ is obtained. The obtained effective permeation coefficients, $\bar{B}$, for each gas, change linearly with the mean pressure $\bar{P}$. It also follows that in coordinates $\bar{B}/K$ versus $\bar{p}/(8K\mu)$ points for different permeation gases should fall on the same straight line with intercept $<r>_\psi$ and slope $<r^2>_\psi$.

$$\frac{\bar{B}}{K} = <r>_\psi + <r^2>_\psi \frac{\bar{P}}{8K\mu} \qquad (16)$$

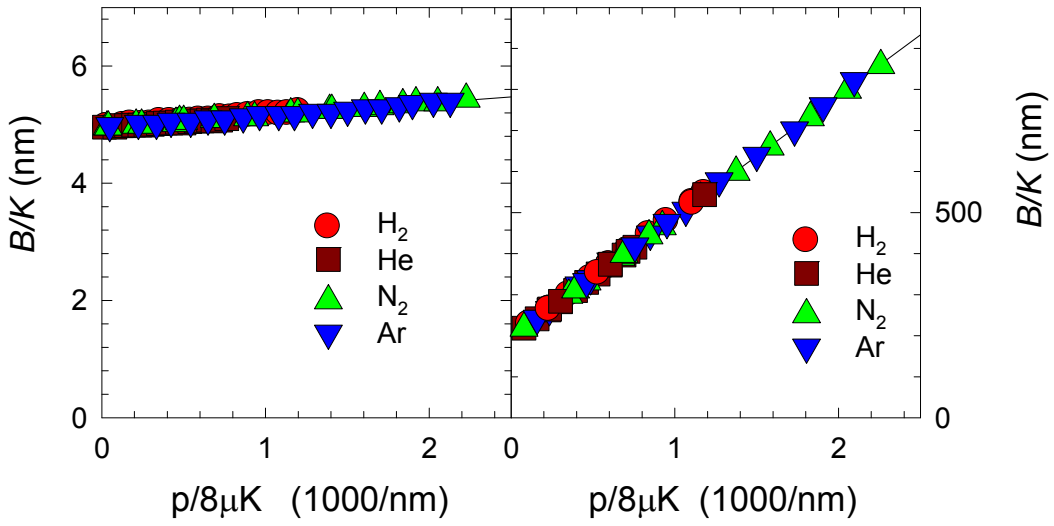

Fig. 6 Comparison of of $\bar{B}/K$ on $\bar{p}/(8K\mu)$ dependences for two porous samples with different pore-size distribution [O16]

In Fig 6, the dependence of $\bar{B}/K$ on $\bar{p}/(8K\mu)$ is shown for two porous samples with different pore-size distribution. It is seen that experimental data comply very well equation (16).

3.4.2 Dynamic cell

After evacuation both compartments are filled with permeation gas up to initial pressure P^o. At run start the gas pressure in the upper cell compartment is increased to pressure P^U and kept constant. The pressure transducer in the lower compartment follows the increase of pressure P(t) up to P^o. The procedure is repeated for several pressures P^o and for other permeating gases. There are existed two solutions; simplified and full solutions [O16].

The very satisfactory agreement of fit for full- and simplified solutions is illustrated in Fig. 7 (for clarity the plot of simplified solution is shifted along the t-axis of the 100 s forwards). It affirms the excellence of data acquisition, reproducibility as well evaluation [O24].

Pure gas flow-rate under a controlled pressure gradient through the pelleted porous material can be studied in the pseudo-stationary cell as well as the dynamic permeation cell. Both arrangements allow evaluation of the two transport parameters $\langle r \rangle_\psi$ and $\langle r^2 \rangle_\psi$ together with the effective permeation coefficients.

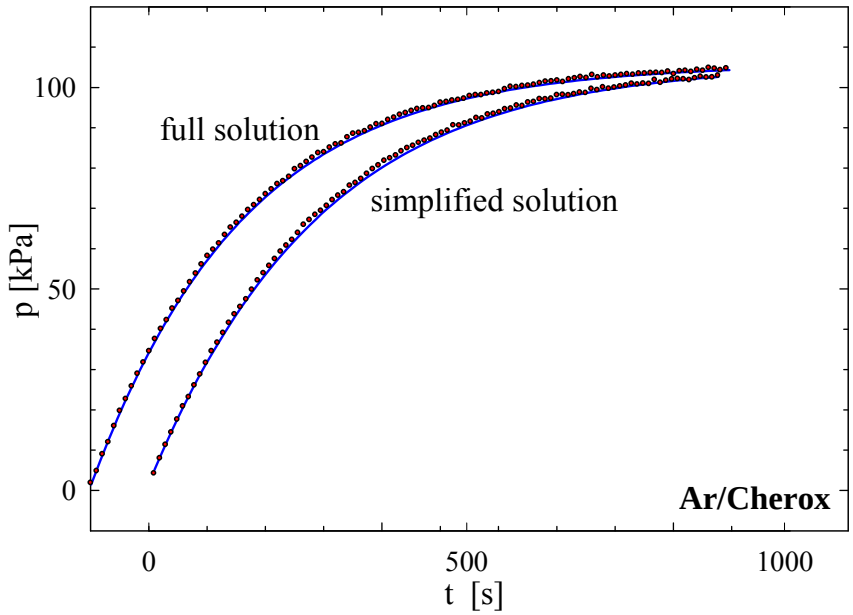

Fig. 7 Agreement of fit for full- and simplified solutions (for clarity the plot of simplified solution is shifted along the t-axis of the 100 s forwards) [O24].

3.5 Combined diffusion and permeation gas transport.

It is often believed that when a porous solid filled with a gas or a gas mixture is suddenly placed in another gas or gas mixture environment the gas transport in the pores is purely diffusional, i.e. the situation in pores is isobaric. Similarly, isobaric conditions in pores are assumed during e.g. a catalytic reaction taking place on pore walls under steady-state conditions. In general this is, however, not true. Isobaric diffusion in pores is possible only when the conditions of the Graham law are fulfilled. Nevertheless, this law is violated during the dynamic process of changing the composition of the gas (gas mixture) surrounding the porous solid. During a catalytic reaction the molar flux densities of gas mixture components are, obviously, related by the reaction(s) stoichiometry and not by the Graham law. Violation of the Graham law is reflected by a spontaneous change (increase/decrease) of the total pressure in different places of pores. Under dynamic conditions this pressure change is also time dependent. This was first experimentally verified by Asaeda et al. [59] in their study of inert gas transport ($H_2/N_2/Ar$) in a bed packed with fine glass powder.

We experimentally confirmed [O9] that under dynamic conditions the countercurrent transport of binary and multicomponent gas mixtures through a porous medium is accompanied by a spontaneous temporary build-up of pressure inside the porous medium. If a lighter gas replaces a heavier gas the pressure increases and *vice versa*. The larger the difference between molecular weights of the transported gases the larger the change of the pressure. If one of the gases in the binary case is replaced by a binary mixture (i.e. transport in a ternary gas mixture) the pressure extremes smoothly interpolate between the limiting binary cases. Thus, in addition to the diffusion transport (with mole fraction (i.e. composition) gradient as the driving force, dy_i/dx) the permeation transport (with totals pressure gradient as driving force, dp/dx) starts to operate and has to be taken into account. Possible solution seems to be the determination of diffusion or permeation transport (transport parameters) by independent diffusion or permeation measurement, e.g. by chromatographic method which guarantees pure dynamic diffusion.

The more complicated seems to be situation when also adsorbable gases are applied [O12]. In such cases the agreement between calculations and experiments is not satisfying. It can be caused, among other things, by capillary condensation of adsorbable gas in pores. Therefore the acceptable simulation of pressure responses can be achieved when adsorption kinetics is taken into account. Probably inclusion of surface diffusion of the adsorbable component would predict more marked pressure changes than experimentally determination.

Investigation of the dynamics of gas transport in porous solids has an impact on many chemical engineering situations. Start-up and shut down

conditions of switch-off catalytic reactors, adsorption processes on porous adsorbents and random steady-state fluctuations in these stages of processes can be named as examples. The knowledge of the qualitative features of the combined transport and the ability to describe its dynamics is of basic importance for the process design and choice of optimum reactor and/or adsorber regimes.

We confirmed O12 that under dynamic conditions the countercurrent transport of binary and multicomponent gas mixtures through a porous medium is accompanied by a spontaneous temporary build-up of pressure inside the porous medium. This fact must be taken into account in the many chemical engineering processes. Possible solution can be the independent determination of the diffusion and permeation transport.

4 Chromatographic methods – dynamic diffusion

The subject of this chapter has been solved in the scope of projects A4072404 (Diffusion Coefficients and Other Transport Characteristics of Specially Shaped Porous Supports and Catalysts) and P1-010-912 (Physical Background of Modern Technologies), and is based on results summarized in articles O6, O8, O29, O33, O39.

Mass transport resistance in the pore structure has been one of the important research fields for many years [60-64], because for modern chemical and biochemical research knowledge of effective diffusion coefficients, textural properties as well as transport characteristics is indispensable.

The majority of these studies, including all above described systems, deal with porous materials of well defined shapes (cylindrical pellets, membrane discs, etc.). This results from the fact that the porous material must be mounted into the measuring cells. In order to increase the outer surface to volume ratio of porous particles a new generation of porous (catalyst, adsorbents, etc.) particle shapes was introduced in chemical industry. Particles are shaped as starcat, starrings, trilobes, polylobes, quatrolobes, irregular spheres, lumps, cylindrical extrudates, Rashog rings, spheroids etc. Such porous particles cannot be mounted in permeation and/or diffusion cells and the only possible way to determine transport parameters is to use a method that can work with ensembles of porous pellets. The only method is the chromatographic technique, well established by [65,66], which permits to study diffusion under dynamic conditions. Porous particles can be packed in the column either as a wide bed (with the ratio of column to particle diameter at least 1:20) or randomly, one by one, with column diameter only slightly larger then particle diameter. This arrangement is known as Single Pellet String Column (SPSC) [67] and has the following advantages: low carrier gas consumption; diffusivities are averaged over many pellets; simple equipment; quick data acquisition. Therefore, the chromatographic technique can be used

for determination of the transport parameter and/or intraparticle effective diffusivities [O75,68-74].

4.1 Single Pellet String Column

In SPSC arrangement high linear carrier-gas velocities - which suppress the mass transfer resistance of the laminar film around particles and tracer peak broadening due to axial dispersion – can be easily attained. This is significant when inert (nonadsorbable) gases are used as tracers, which move through the column with the high carrier-gas velocity. The use of inert tracers prevents their adsorption and the possible surface diffusion, which obscures the effective diffusion coefficients [75] and transport characteristics. Another advantage of the SPSC arrangement is the averaging of obtained transport characteristics over many pellets present in the column. In addition: SPSC guarantees low carrier gas consumption. SPSC set-up is schematically shown in Fig. 8.

Today the Kubín–Kučera model [76,77]] is applied almost exclusively for the description of processes taking place in a column packed with the tested porous material after the pulse of a tracer-gas (T) is injected into the carrier-gas (C), which flows steadily through the column. Effective diffusivities and other transport parameters are then evaluated from tracer response curves at the column outlet. Instead of the frequently used matching of moments of the tracer response, the time-domain matching [O29, O33, 78,79], i.e. finding parameters for which the calculated tracer response best agrees with the experimental response curve.

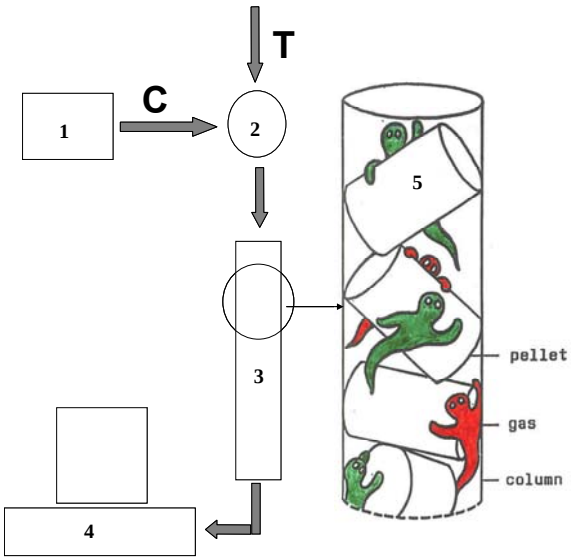

Fig. 8 SPSC set-up, 1 – gas source, 2 - six-ways valves, 3 – column, 4 – data logger ,C – carrier gas, T – tracer gas [O29]

Model parameters are as follows:

Pe is the Peclet number (Pe = vL/E and E is the axial dispersion coefficient),
t_{dif} denotes the diffusion time of the tracer in the pore structure of a pellet, $t_{dif} = R^2\beta/D_{TC}$ (with the radius of the pellet equivalent sphere, R),
δ_o is the tracer adsorption parameter $\delta_o = \gamma(1 + K_T)$, and $\gamma = \beta\ (1\text{-}\alpha)/\alpha$,
β is the pellet porosity and α is the column void fraction (interstitial void volume/column volume),.
γ, is the pore volume per unit interstitial volume. For an inert tracer $K_T = 0$ and $\delta_o = \gamma$.
Q is a normalization constant defined so that at the calculated SPSC response maximum tracer concentration equals unity, $c(t_{max}) = 1$. The intracolumn processes are described correctly but the effects of processes upstream and downstream of the column (extra column effects - ECE) are neglected. ECE were firstly defined in article [O6]. For their evaluation a new special experimental set-up and measurement method were designed, constructed and applied. Thus, peak distortion because of the sampling valve, tube connections between sampling valve, column and detector, detector itself is not accounted for. Obviously, the usual neglect of these effects significantly biases the obtained t_c and Pe parameters.

The chromatographic technique in the Single Pellet String arrangement (SPSR) seems to be a suitable technique for determination of the transport parameter and/or intraparticle effective diffusivities for a new generation of porous particles with irregular shapes which have been introduced in chemical industry. The carrier-gas flows steadily through the packed chromatographic column and into this stream the tracer-gas is injected. Processes taking place in the chromatographic column which influence the peak shape can be described by the model parameters.

4.2 Data evaluation by convolution theorem

In the time-domain matching it is possible to include these effects through the application of the convolution theorem. This requires, besides the knowledge of the experimental system response, also the knowledge of the ECE response. The ECE response can be replaced by experimental system responses for two columns with different length. The convolution theorem states that the column response, c(t), is given by the convolution integral

$$c(t) = \int_0^t g(t-u)\, h(u)\, du,$$ where h(t) is the column impulse response and g(t) describes the shape of the signal entering the column instead of the Dirac delta function impulse. In linear systems it is immaterial if the ECE are distributed in different places of the system or if they are concentrated in one place and in what order they are arranged. Therefore, it is possible to use the experimental responses for the shorter column as g(t).

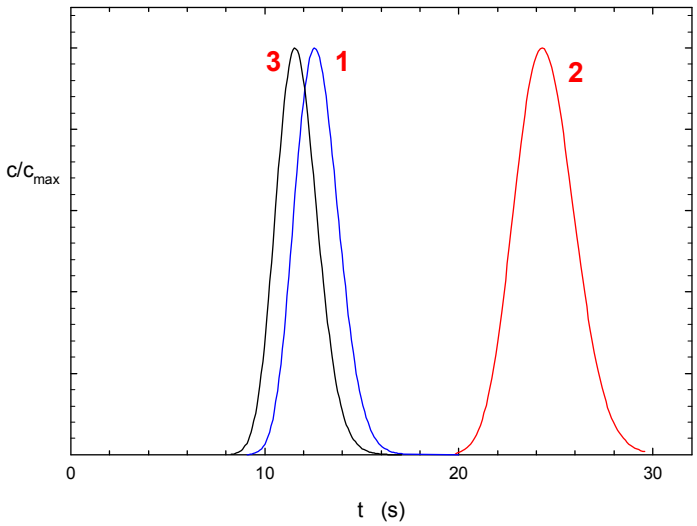

Fig. 9 The application of convolution method; 1 - the experimental response of a shorter column (0.5 m), 2 - the experimental response of a longer column (1 m) and 3 is the calculated impulse response for a column with length 0.5 m [O29]

The application of convolution integral is demonstrated in Fig. 9, where 1 is the experimental response of a shorter column (0.5 m), 2 is the experimental response of a longer column (1 m) and 3 is the calculated impulse response for a column with length: 1 m – 0.5m = 0.5 m. Because the length of longer column is double of the length of shorter column, the difference between peaks 2 and 3 belongs to extra column effects.

4.3 Axial dispersion evaluation

In original evaluation system used in [O8] the parameter t_c was obtained from the SPSC volume, V_c, bed porosity, α, and the carrier gas flow-rate, v, as $t_c = \alpha V_c/v$. Thus, only t_{dif}, Pe and δ_o had to be obtained by matching. Unfortunatelly, the Peclet numbers obtained by three parameters matching agreed with the Peclet numbers from matching of responses of SPSC packed with nonporous cylindrical pellets only at low carrier gas velocities. At higher carrier velocities the Peclet numbers in SPSC packed with porous pellets were significantly higher than in SPSC packed with nonporous particles. Thus, matching of three parameters together causes high uncertainty in parameters determination.

From that reason a new unique system of parameter evaluation was formulated [O75]. Axial dispersion (Peclett number) was evaluated firstly for nonporous pellets, thus parameter t_{dif} was eliminated. Moreover, the strict application of nonadsorbable gases eliminated also adsorption parameter δ_o. For nonporous packing (nonporous particles with the same shape as porous

ones) the only two unknown parameters remain, Pe and t_c, which are not correlated and their matching is quick and straightforward.

In order to remove the column length, L_c, from Pe, $Pe = v L_c/E_{TC}$, it is possible to use the Bodenstein number, Bo, which contains the packing particle size, d_p, as the characteristic dimension $Bo = v d_p/E_{TC}$ instead of the Peclet number. Hence $Bo = Pe (d_p/L_c)$. For spherical pellets the sphere diameter and for cylindrical pellets the equivalent sphere diameter (sphere diameter with the same volume/surface ratio) can be used [see O29]. The product of Reynolds and Schmidt numbers, ReSc, was used as the measure of carrier-gas velocity $ReSc = vd_p/\mathcal{D}^m_{TC}$.

It was also verified that for packing pellets placed into the column one by one, quite regular and reproducible column packing was obtained. For spherical pellets with $d_p > d_c/2$ the packing pattern is, obviously, unique. With cylindrical pellets different packing patterns can be obtained, depending on the ratio of pellets height and diameter, H/D, as well as on the equivalent sphere diameter d_p. The void volume of the packed column is, nevertheless, quite reproducible. As we reported in [O29] six fold repacking a column with cylindrical pellets (H/D = 1, $d_p/d_c = 0.63$) resulted in the column void fraction $\alpha = 0.60$ with the relative standard deviation of only 0.4 %.)

For spherical pellets the Bo - ReSc dependence is affected by the pellet/column diameter ratio, d_p/d_c. For cylindrical pellets their height/diameter ratio, H/D, plays an additional role. To characterize more complicated particle geometries it is possible to use the sphericity, φ, defined as the ratio of the surface area of the sphere of the same volume as the particle and the surface area of particle. Thus, for spherical particles φ = 1 and for cylindrical pellet $\varphi_{cylinder}$ is given as

$$\varphi = \left(\frac{18(H/D)^2}{(1+2(H/D))^3} \right)^{1/3} \tag{17}$$

Edwards and Richardson [81] correlated axial dispersion results for packed beds from numerous sources by an equation of the form

$$\frac{1}{Bo} = \frac{\gamma}{ReSc} + \frac{\lambda ReSc}{\beta + ReSc} \tag{18}$$

To correlate SPSC data for *spherical and cylindrical pellets* in [O66] we modified this correlation by introduction of a term for the ratio d_p/d_c and another term for cylinder sphericity from equation (17)

$$\frac{1}{Bo} = \frac{\gamma}{ReSc} + \frac{\lambda_o \left[1-\lambda_1(d_p/d_c)\right]\left[1+\lambda_2(1-\varphi)\right] ReSc}{\beta + ReSc} \tag{19}$$

Naturally, for spherical pellets for which φ = 1, this equation simplifies to Equation (20)

$$\frac{1}{Bo} = \frac{\gamma}{ReSc} + \frac{\lambda_o\left[1-\lambda_1(d_p/d_C)\right]ReSc}{\beta+ReSc} \qquad (20)$$

Equation (20) was verified for $d_p/d_c \in (0.56, 0.8)$ and the reasonable quality of fit was obtained. Nevertheless for spheres with diameters approaching the column diameter ($d_p/d_c \rightarrow 1$) problems arising during recording of SPSC responses was detected. The reason is probably the more complicated hydrodynamics of gas flow through the very narrow gap between packing and inner column wall.

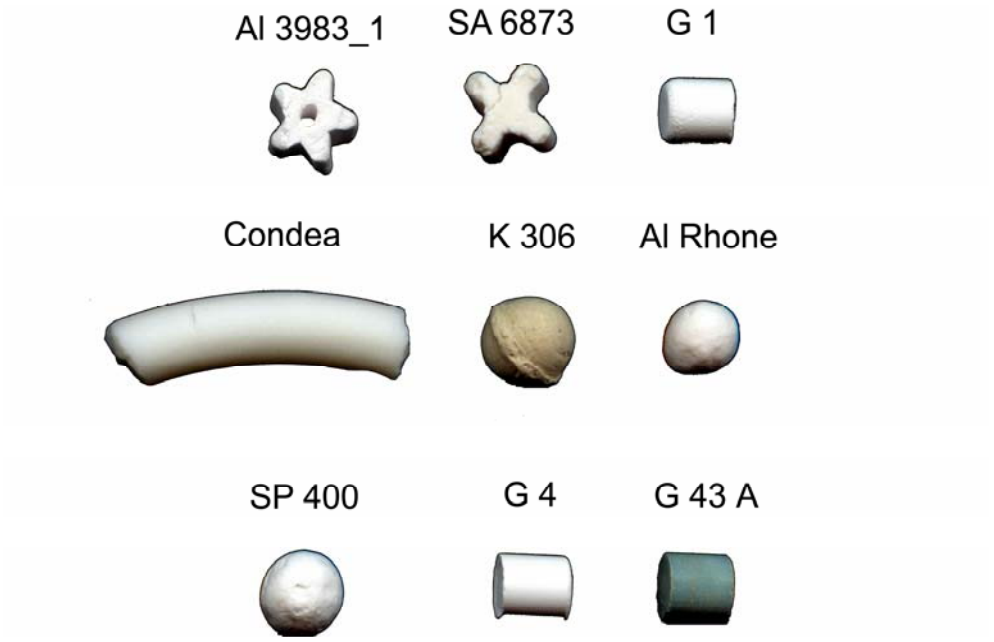

Fig. 10 Shapes of used porous materials [O33]

To verify validity of Eq. 19, evaluated for cylindrical pellets for a wide range of non-standard pellet shapes and sizes [O66], it was necessary to obtain non-porous twins of unusually shaped porous pellets (stars, lumps, irregular spheres, cylindrical extrudates, trilobes etc.) that could be used for independent determined of axial dispersion characteristics. The special liquid (Porofil) was used for pore blocking [O33] to hinder the access of tracer- and carrier-gases into pores and, thus, to remove the intraparticle pore-diffusion process. In this way, the soaked-up pellets behave as non-porous ones.
Comparison of experimental and calculated Bo-ReSc dependences for 6 types of non-porous cylindrical pellets and 9 types of porous pellets with pores blocked by Porofil (shapes see in Fig 10) are shown in Fig 11. Similarly as for spherical pellets the fit which covers the intervals $d_p/d_c \in (0.35, 0.87)$ and $\varphi \in (0.42, 0.89)$ is reasonable good.

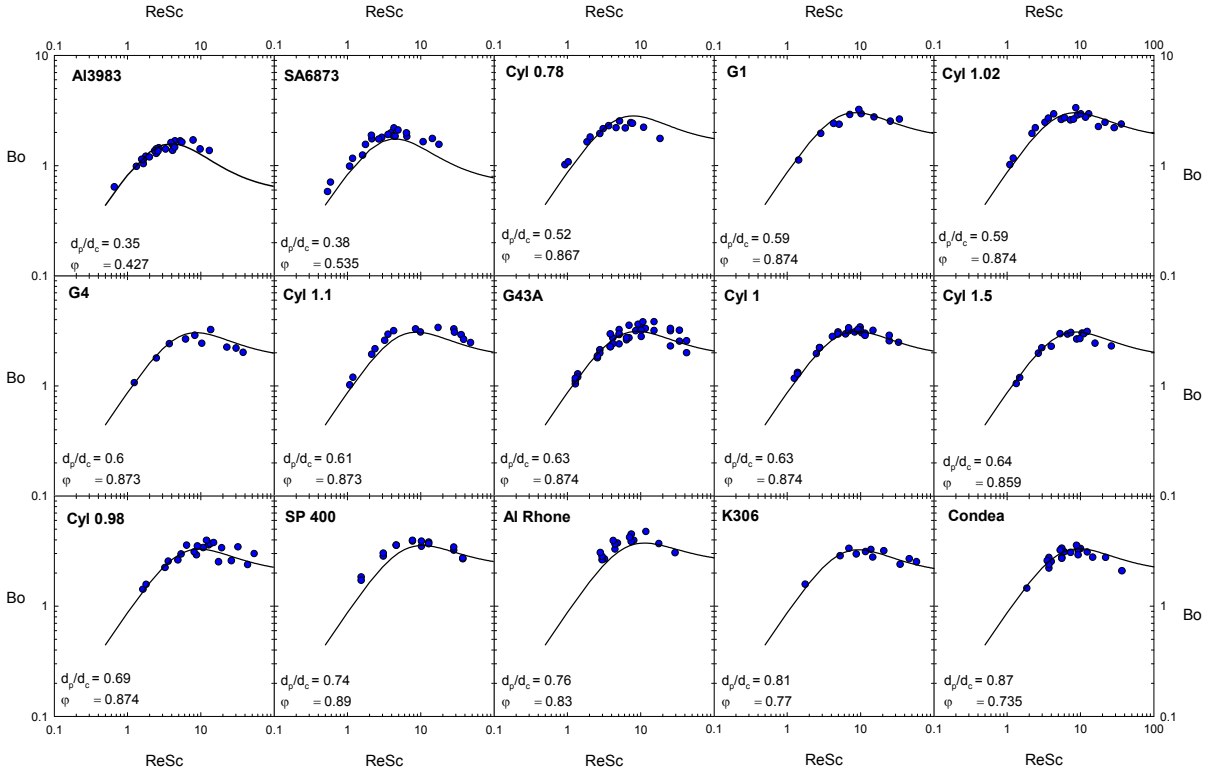

Fig. 11 Bo – ReSc dependences for cylindrical and irregular pellets; points – experimental; lines - calculated [O33]

It is easily seen that all dependences Bo(ReSc) pass through a maximum at $ReSc_{opt}$, which is the great of importance fact. Hence, there exist carrier-gas linear velocities, $v= (\mathcal{D}_{TC}/d_p)\, ReSc_{opt}$, for which the axial dispersion, E_{TC}, is the lowest. This velocity is then suitable for determination of pore-diffusion, since the pore-diffusion parameter is least affected and it is determined with highest confidence.

The corresponding $ReSc_{opt}$ product follows from the condition d(Bo)/d(ReSc) = 0, Equation (19), i.e.

$$Re\,Sc_{opt} = \frac{\sqrt{\gamma\beta}}{\lambda_o\left[1-\lambda_1\left(d_p/d_c\right)\right]\left[1-\lambda_2\left(1-\varphi\right)\right]-\sqrt{\gamma/\beta}} \qquad (21)$$

Use of the obtained correlations for axial dispersion in the SPSC arrangement can improve significantly the confidence of pore-diffusion characteristic evaluated from responses of *SPSC packed with porous pellets of unusual shapes.* Pellets of these shapes manifest now growing practical importance and it is very difficult to obtain for them effective diffusion coefficient and/or transport characteristics by other experimental procedures.

For evaluation of effective diffusion coefficients and/or transport characteristics of porous materials packed in the chromatographic column the time-domain matching was applied. The convolution theorem was employed

to include effects (characterized by the model parameters), which influence the chromatographic peak, into the evaluation process. To increase the accuracy of estimated parameters the axial dispersion was evaluated first for nonporous pellets by the application of nonadsorbable gases. Next, an equation for evaluation of the axial dispersion was formulated based on the experimental results. Its validity was confirmed not only for spherical and cylindrical pellets but also for a wide range of non-standard pellet shapes and sizes. Moreover, it was also confirmed that for any pellets the carrier-gas linear velocity for which the axial dispersion is the lowest exists. Thus, this velocity is then the best for determination of pore-diffusion characteristics.

4.4 Effective diffusion coefficients

Using the independently obtained Peclet number decreases the number of parameters for matching of the porous packing response from four ($t_{dif,}$ Pe, δ_o, t_c) to three ($t_{dif,}$ δ_o, t_c). The tracer adsorption parameter, $\delta_{o,}$ can be determined from the difference of first absolute peak moments for two column lengths, $(\mu'_1)_{col1}$, $(\mu'_1)_{col2}$. Thus, only t_{dif} and t_c have to be determined by the time-domain matching; and these parameters are not correlated [O8].

The convection- , t_c, and diffusion-, t_{dif}, times followed from the time-domain fitting. The effective diffusivity coefficient, D_{TC}, that includes contributions from the Knudsen diffusion mechanism and molecular diffusion mechanism, can be obtained from $t_{dif} = (d_p/2)^2\varepsilon/D_{TC}$. MTPM parameters, $\langle r\rangle\psi$ and ψ, are then determined from the Bosanquet formula (22)

$$\frac{1}{D_{TC}} = \frac{1}{\langle r\rangle \psi K_T} + \frac{1}{\psi \mathcal{D}_{TC}^m} \tag{22}$$

which includes the molecular diffusion coefficient of the pair C-T, $\mathcal{D}_{TC}^m$, and the tracer Knudsen constant $K_T = (2/3)\sqrt{(8R_gT/\pi M_T)}$ with the universal gas constant, R_g, temperature, T, and tracer molecular weight, M_T. Equation (51) can be rearranged into the form (23), which permits data evaluation, e.g. by the easy graphical method.

$$t_d K_T = \frac{(d_p/2)^2\ \varepsilon}{\langle r\rangle\psi} + \frac{(d_p/2)^2\varepsilon}{\psi}\frac{K_T}{\mathcal{D}_{TC}^m} \tag{23}$$

The obtained diffusion times, t_{dif}, are plotted in co-ordinates $t_{dif}K_T$ versus $K_T / \mathcal{D}_{TC}^m$. Transport parameters, $\langle r\rangle\psi$ and ψ, are evaluated from the straight-line slope and intercept. Furthermore, it is possible to determine the ratio of contributions of Knudsen and bulk diffusion mechanisms.

Thanks to the independently obtained Peclet numbers the diffusion parameter could be determined with high accuracy from the time-domain fitting. Then, the effective diffusivity coefficient together with transport parameters, $\langle r\rangle\psi$ and ψ were evaluated and the ratio of contributions from the

Knudsen diffusion mechanism and molecular diffusion mechanism was determined. The significant decrease of the Knudsen diffusion flux with growing pore sizes was confirmed for porous material with various structures.

5 Comparison of methods for characterization of porous solids

The subject of the following chapter has been solved in the scope of projects A4072915 (Complex Textural Characterization of Porous Solids Regarding the Mutual Relationship of Different Methods) and GA104/01/0546 (Correct Characterization of Porous Solids for Mass Transport in Pores) it is based on results summarized in articles O7, O13, O22, O25, O40, O75 and doctoral thesis (K. Soukup, Multiphase diffusion in pores and validity of Graham law, 2006).

All the above described methods provide results on textural and transport characteristics relevant to chemical/biochemical processes. Nevertheless, one of the important aspects is determination of the mutual correlation of individual methods as well as evaluation of their validity with respect to the complicated material structure. Based on this knowledge it is possible to make reliable predictions and the described material characteristics can built the necessary chemical-reaction-engineering background for complex description of transport-affected chemical/biochemical processes.

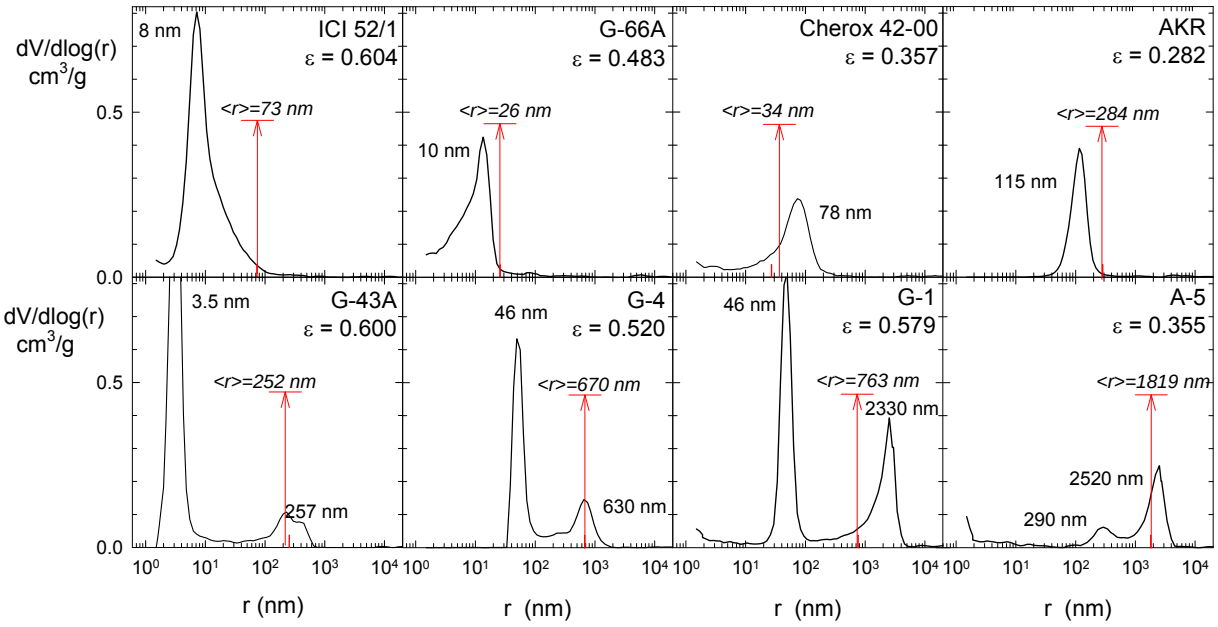

Fig. 12 Comparison of the pore-size distributions from mercury porosimetry (solid lines) with mean pore-radii from diffusion measurements (red arrows) [O25]

Firstly, the basic comparison between textural and transport characteristics has been done [O39]. The mean pore radii for porous materials

with the various bidisperse pore structures (obtained from diffusion measurements) are compared with pore-size distributions (PSD) from mercury porosimetry and permporometry, see data given in Fig 12. For all samples (for description see Table 1) the mean pore radii are either positioned between peaks of mercury pore-size distributions closer to the peak of wider pores or agree with the peak for wider pores. It follows then, that the gas transport takes place predominantly through wider pores and the role of narrower pores depends on their size and number. This fact was corroborated in all our other studies [O13,O15,O34].

It is obvious that although the classic textural analysis methods (e.g. high pressure mercury porosimetry, physical adsorption of inert gases) provide consistent information on texture characteristics, they take into account all pores and partition into transport-pores (pores through which the decisive part of mass transport takes place) and blind pores (which contain the surface area but are not active in mass transport) is not feasible. Therefore, information on pore-size distributions (PSD) obtained from classic textural analyses cannot, in general, be used for rational prediction of mass (e.g. gas) transport in any processes where only the transport-pores are significant and knowledge of transport-pore size distribution is essential.

Thus, the liquid-expulsion permporometry is the only standard method that can give the transport pore PSD curves. This method can provide reliable data [O34], however, it is necessary to take into account its limitations; the necessity of filling pores by suitable liquid, the long stabilization period for thicker materials, or the application very high pressures to expel liquid from pores under 50 nm.

Comparison of transport parameters obtained by the dynamic diffusion (the dynamic chromatographic technique) with transport parameters obtained by the steady- state diffusion (the steady-state binary/multicomponent gas counter-current diffusion) was also thoroughly studied. One would expect that transport parameters evaluated by both diffusion methods could be in a good agreement. It is mostly true for the evaluated mean transport-pore radii [O34]. Nevertheless, the transport parameter, ψ, from counter-current diffusion is approximately three times higher then from the chromatographic technique. The explanation might partly lie in the definition of this parameter: ψ is defined as the ratio of transport-pore porosity to transport-pore tortuosity. The transport-pore tortuosity depends on the actual length of diffusion trajectory through the pellet, which differs in counter-current diffusion and the chromatographic technique. While in the (steady-state) diffusion method pores branching from transport-pores are of no significance, in the (dynamic) chromatographic technique they effectively lengthen the diffusion pathway. Another effect that can play partly/in addition a role is the fact that in the SPSC the whole external surface is available for transport inside and outside of the porous pellet. This is not true for cylindrical pellets mounted into the

diffusion cell; here only the cylindrical pellet bases are exposed to diffusing gases. It is noticeable that transport parameters are effective values, which incorporate all details not explicitly defined in the model. The unincorporated details, obviously, differ for both types of processes.

For comparison of transport parameters obtained from diffusion and permeation measurements porous materials with various pore structures were used. To exclude the influence of material geometry the same pellets mounted into the discs were used for both measurements. Deviations between transport parameters $(\langle r\rangle\psi)_d$ and $(\langle r\rangle\psi)_p$ (index "d" stands for diffusion and "p" for permeation) lay between 0 - 10% rel. However, the mean transport-pore radii from permeation measurements, $(\langle r\rangle)_p$, were nearly in all cases slightly higher than from diffusion measurements, $(\langle r\rangle)_d$. The reason could lie in the method used for $(\langle r\rangle)_p$ determination. From directly evaluated $(\langle r\rangle\psi)_p$ $(\langle r\rangle)_p$ was calculated with the use of $(\psi)_p$, which followed from $(\langle r^2\rangle\psi)_p$ and $(\langle r\rangle\psi)_p$. This approach assumes that $\langle r\rangle^2 = \langle r^2\rangle$ which is true only for (infinitely) thin transport-pore radii distributions. Therefore, values of $(\langle r\rangle)_p$ and, consequently, of $(\psi)_p$ have to be looked upon with substantial caution. Moreover, the uncertainty of $(\langle r\rangle\psi)_p$ and $(\langle r^2\rangle\psi)_p$ depends on the relative role of Knudsen transport and molecular transport.

All our studies point to the main conclusion that the best way for determination of relevant characteristics for the chemical-reaction-engineering background is the combination of techniques. Of course, sufficient view from above on the material characteristics evaluation and judgment is indispensable.

6 Chemical engineering applications of results

The topics of this chapter have been solved in the scope of projects RFCR-CT-2007-00006 (Hydrogen Oriented Underground Coal Gasification for Europe), RFCR-CT-2010-00002 (Hydrogen Oriented Underground Coal Gasification for Europe - Environmental and Safety Aspects), FR-TI1/059 (Utilization of combined thermal desorption and catalytic oxidation methods for the solid waste decontamination), TA01020804 (Removal of endocrine disruptors from wastewater and drinking water using photocatalytic and biological processes) and it is based on results summarized in articles O36, O51, O60 and O76 and results obtained thanks to three PhD themes (not defended yet; S. Krejčíková, Preparation and characterization of the metal oxide thin layers, M. Morozová, Photochemical processes on the titania thin layers and L. Spáčilová, Water purification by photocatalytic processes).

The last chapter is devoted to the practical utilization of describe methods. To show their wide practical impact six examples from different areas of chemical engineering are presented.

6.1 Determination of effective diffusion coefficients of exhaust gases in automotive catalyst

Structured catalyst supports are widely used in automotive exhaust gas converters [O36]. Small sized channels are contained in monoliths to provide large surface area of the car catalytic convertors. Typically both metal and ceramic monoliths are used [83,84]. Ceramic monoliths made from cordierite with square cross-section channels are employed quite extensively because of relatively low production costs [85,86]. The active catalyst is supported (washcoated) onto the monolith by dipping it into slurry containing the catalyst precursors. A commonly used washcoat material is γ-Al_2O_3 with a typical surface area of 100 – 200 m^2/g. The excess of the deposited material (washcoat) is then blown out with hot air and monolith is calcined to obtain the finished catalyst [84,86,87]. This process gives thin washcoat layer; however, it also results in a variation in thickness around the channel perimeter. Although the washcoat layer is thin, pore diffusion can affect monolith performance [88-92], and thus need to be included in any realistic mathematical model. Therefore, it is necessary to have reliable information on the mass transport rate in the porous medium as well as the effective diffusivities of exhaust gases in the washcoat layer.

To obtain the effective diffusion coefficients with relatively high accuracy the chromatographic method was employed. True densities of washcoat samples (which were cut from different positions around the monolith perimeter) vary more then 10%. The chromatographic technique suppressed this problem since the results were averaged over many pellets (more then two hundred pellets were packed in columns). The obtained transport characteristics [O36] were used for estimation of effective diffusion coefficients for CO-N_2, CH_4-N_2 and C_3H_6-N_2 pairs, which are of interest world-wide. Such coefficients are only rarely found in the literature.

6.2 Description of gas transport in strata during underground coal gasification

The underground coal gasification (UCG) is a method for in-situ coal conversion into a combustible gas with a high-energy value [O51].UCG minimizes the environmental damages in comparison with the traditional coal mining techniques [93]. Several modifications of UCG [94-96] were suggested and tested for in-situ production of hydrogen through gasification of the unmineable coal seams not feasible by the modern classic mining technologies. Especially for the deep coal seams this method seems to be very promising.

During UCG the injected oxidizing mixture (oxygen, air, steam/oxygen or steam/air) reacts with coal to form a product gas which is subsequently brought to the surface, then cleaned and used as a syngas both for power and

fuels production (e.g. hydrogen, synthetic natural gas or liquid fuels) [93]. In any case the gases produced in the reaction zones could leak through overburden strata. Therefore, the knowledge of the gas transport rates through porous layers is essential for project applicability to a wide range of geological conditions. Moreover, the coal seams are often situated near the densely populated areas which could cause a serious problem during UCG without precise appraisal of the gas transport front in time.

The direct proportionality of the effective permeability coefficient to the effective squared mean pore radius was confirmed. At the same time the effect of evaluated pore sizes on rate of gas front movement was lower than the effect of the pressure increase. It was also found that the movement of the gas front for individual gases corresponds to gas viscosities; the higher the gas viscosity the lower the gas transports rate. The front of individual gases will move in the order hydrogen > ammonia > methane > hydrogen sulfide > carbon dioxide > carbon monoxide. The rate of the hydrogen front movement is approximately only twice higher than the movement of CO_2 front; nevertheless, H_2 front appears at the distance lower than one kilometer for the highest evaluated pressure after some years.

6.3 Evaluation of gas transport through nanofiber membranes prepared by electrospinning

In recent years the practical application (e.g. catalysis, filtration, tissue engineering, wound care) of nanofiber membranes has increased tremendously [O60]. By electrospinning process, that is the most common technology used for nanofiber preparation [97-101], the prepared nonwoven mats include the submicron fibers with large surface area per unit mass and also very high macroporosity. Density of these materials is usually very low (commonly 0.01–0.1 g/cm^3). Especially, in heterogeneous catalysis nanofiber systems (membranes) seem to be promising porous carriers for immobilization of homogeneous catalysts based on the biopolymer compounds [97,102,103]. Immobilization on the nonwoven mats allows an accurate controlling of the catalytic activity and accessibility of the catalyst as well as its recovery from the reaction mixture. Sufficiently high specific surface area (ranging from 1–35 m^2/g in dependence on the fibers diameter) together with generally low transport resistance of nanofibrous membranes competes with traditionally supported porous catalysts. Nanofibrous membranes (Fig. 13) seems to be promising supports owing to their fine porous structure, a good pores interconnectivity, a high specific surface area and appropriate transport properties (generally low diffusion resistance). It must be noted that membranes prepared from the layered nanofibers reveal enhanced transport properties useful for catalytic processes as well as various separation systems. These parameters depend on the fiber diameter, thickness of a membrane, weight per a unit area, etc.

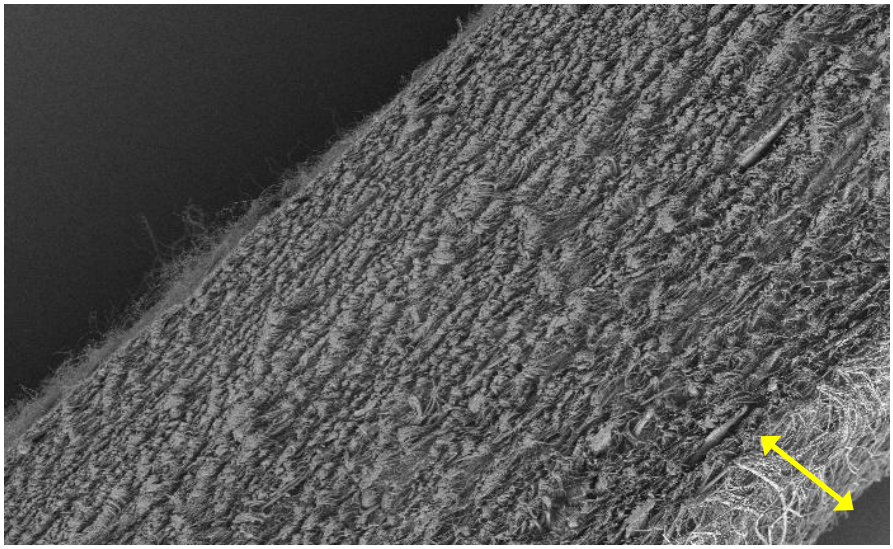

Fig. 13 Nanofiber polystyrene membrane; the thickness is defined by the yellow arrows

Study was focused on optimization of preparation of polystyrene (PS), polyurethane (PU) as well sandwich PU-PS-PU nanofiber membranes based on knowledge of their structural description and diffusion characteristics. Thus, properties of individual prepared membranes can be optimized with respect to requirements for individual practical utilization. It was found that the diffusion resistance of the polyurethane membrane was much higher than that of the polystyrene membranes of the same thickness. The diffusion flow resistance increased with the membrane thickness in the whole range of areal weights (in kg/m^2) for the polyurethane membranes. On the other hand, it remained nearly unchanged for the polystyrene membranes with three times lower area weight. The diffusion resistance of the sandwich membrane correlates well with the diffusion resistance of the pure PU membrane and the diffusion transport through the PU membrane is the rate determining step. Thus, alternation of PU, PS membrane components together with the PU membrane thicknesses can control adjustment of the PS-PU sandwich membrane permeability.

6.4 Preparation and microstructure optimization of iron oxide pellets for hydrogen storage

There exists a long known approach for hydrogen storage based on the steam iron process. By this method, hydrogen storage can be described as a reduction of iron oxides to metallic iron by hydrogen [O76, 104-106] ($Fe_3O_4 + 4H_2 \rightarrow 3Fe + 4H_2O$) and hydrogen production is achieved through the oxidation of iron by steam water ($3Fe + 4H_2O \rightarrow Fe_3O_4 + 4H_2$). The redox cycle of iron oxides can be applied as a new method of storage and supply of

hydrogen. In this method hydrogen is not stored directly, because redox cycle of iron/iron oxides works apparently as a medium for hydrogen storage. Theoretical amount of hydrogen stored as Fe metal is 4.8 wt. %. At high temperature and pressure the reaction equilibrium is shifted to the right (i.e. hydrogen storage), at lower temperature and pressure the equilibrium is shifted to the left (i.e. hydrogen recovery). High repeatability of these cycles can be achieved by addition of various additives (e.g. Al_2O_3) to iron.

The iron oxides are prepared by precipitation of aqueous ferric nitrate. The addition of aluminium oxide into iron oxides prevents the sintering of metal iron and/or iron oxides during repeated redox cycles. Chromatographic technique together with classic texture analyses were employed to find the optimal porous structure based on the amounts of alumina additive together with the optimal calcination temperature for pellets preparation. It was found that pellet stability that is essential for repetition of redox reaction and thus, process successfulness, depends on the material sintering during process (and thus on its texture properties) and can be crucially effected by initial calcination temperature.

6.5 Tailoring of porous materials for environmental applications

The necessity to find alternative solutions for environmental protection leads to the development and use of new technologies. Photo-catalysis using semiconductor particles have found increasing concern in the solution of global pollution problems [107-109]. Compared to other photocatalysts, TiO_2 and/or doped TiO_2 appear to be the most promising material not only in advanced oxidation photo-catalytic processes (AOP) [110-112].

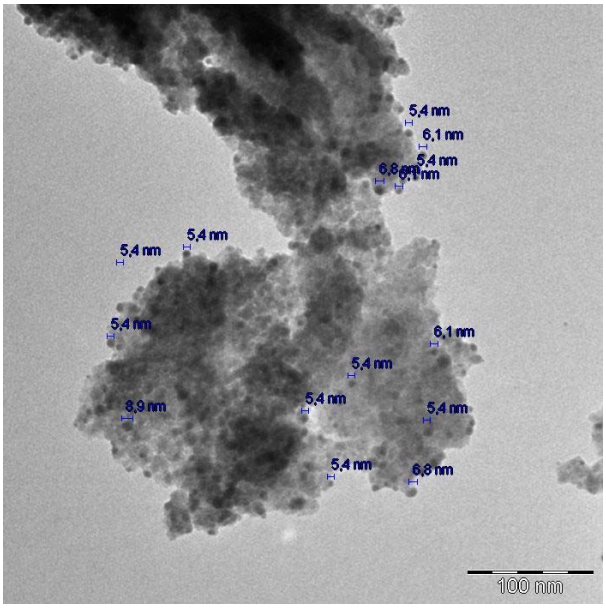

Fig. 14 TEM micro-photograph of the TiO_2 crystallite structure

It is well established that in the presence of UV light titanium oxide and related nanostructure materials can create very active species that are able to restore and preserve a clean environment by decomposing harmful organics, killing bacteria and viruses and being easily self-cleaned [113-115].Recent investigation is focused on the preparation of the specially designed photoactive materials and their modified versions with a tailored structure suitable for photo-processes carried out upon illumination in the visible and UV regions of the light. Tailoring of similar materials must be based on the perfect knowledge of material texture.

A set of doped titania photocatalysts (see Fig. 14) with tailored structure was prepared for activity testing in photocatalytic oxidation of 4-Chlorophenol (4-CP) water solution [O72] and photocatalytic reduction of CO_2 [O49, O56, O78]. The important effect of the catalyst composition and structure on the catalytic efficiency was confirmed for both reactions.

Photocatalytic reduction was carried out in the stirred batch annular reactor with suspended catalyst in 0.2 M NaOH solution saturated by CO_2 before irradiation by an 8 W Hg lamp. Dependence of the methane yields (after 24 hours of irradiation) on the particle size in the range 4.5 – 29 nm during photocatalytic reduction of CO_2 was evaluated. The observed optimum particle size was a result of competing effects of specific surface area, charge–carrier dynamics and light absorption efficiency.

Ag doped TiO_2 photocatalysts revealed significantly higher photocatalytic activity than pure TiO_2 or commercial Degussa catalyst. The concentration of 4-CP fell down quickly except for the Degussa catalyst. It was verified that degradation of 4-CP over tailored catalysts can run quickly under so mild conditions (room temperature, pH 7). Thus, the tested reaction system could be promising as the environmentally friendly alternative for wastewater purification.

7 Summary

The thesis summarized research concerning the experimental methods suitable for obtaining material characteristics relevant to chemical engineering aspects of the gas transport in porous solids that was done since 1991. The thesis is based on 78 articles and chapters in books and was supported by seventeen projects from various grant agencies. Evaluation of the individual unique methods together with their theoretical background and the special set-up constructions is described including their mutual correlations in connection with their practical use.

The correct evaluation of texture properties from physical adsorption measurements for nitrogen as well as argon together with the appreciation of individual methods was evaluated and described. The developed unique

permporometry method that enables evaluation of the pore-size distribution of the flow-through pores was also introduced.

Evaluation of transport characteristic relevant to transport in pores inevitable for any prediction or simulation of gas transport in porous solids, is thoroughly discussed. The constitutive equations of two models; the Mean Transport-Pore Model (MTPM) and the Dusty Gas Model (DGM), which describe combined (diffusion and permeation) transport through the porous medium, are collected. Application of Wicke-Kallenbach and Graham diffusion cells as well as the pseudo-stationary and dynamic permeation cells for the transport characteristics and the effective diffusion and permeation coefficient evaluation is shown.

Advantages and disadvantages of the individual methods with respect to their application for chemical engineering calculations, process development and design are described together with their possible impact. Besides that the chromatographic method with the special evaluation system based on the developed interpolation equations that enables determination of the effective diffusion coefficients as well as transport parameters for any shape of porous materials is also introduced, discussed and evaluated together with its impact in the practical use. Finally, the wide impact of the individual methods for the practical application is shown for selected examples from different areas of the chemical engineering.

8 Original papers used in the thesis

O 6 Šolcová O., Schneider P.: Extra-column effects in determination of rate parameters by the chromatographic method. Coll. Czech. Chem. Commun. 61(6), 844-855 (1996).

O 8 Šolcová O., Hejtmánek V., Schneider P.: Determination of effective diffusivities and transport parameters of porous solids in the Single-Pellet-String-Column. Catal. Today 38, 71-77 (1997).

O 9 Hejtmánek V., Čapek P., Šolcová O., Schneider P.: Dynamics of pressure build-up accompanying multicomponent gas transport in porous solids: inert gases. Chem. Eng. J. 70, 189-195 (1998).

O 12 Hejtmánek V., Čapek P., Šolcová O., Schneider P.: Dynamics of pressure build-up accompanying multicomponent gas transport in porous solids: adsorbable gases. Chem. Eng. J. 74(3), 171-179 (1999).

O 13 Šolcová O., Šnajdaufová H., Hejtmánek V., Schneider P.: Textural properties of porous solids in relation to gas transport. Chem. Pap. 53(6), 396-402 (1999).

O 15 Šolcová O., Schneider P.: Transport Characteristics of Porous Solids Derived from Chromatographic Measurements. Stud. Surf. Sci. Catal. 144, 475-482 (2002).

O 16 Čapek P., Hejtmánek V., Šolcová O.: Permeation of Gases in Industrial Porous Catalysts. Chem. Eng. J. 81(1-3), 281-285 (2001)

O 19 Šolcová O., Šnajdaufová H., Schneider P.: Multicomponent Counter-Current Gas Diffusion in Porous Solids: The Graham's-Law Diffusion Cell. Chem. Eng. Sci. 56, 5231-5237 (2001).

O 24 Hejtmánek V., Šolcová O., Schneider P.: Gas Permeation in Porous Solids. Two Measurement Modes. Chem. Eng. Commun. 190(1), 48-64 (2003).

O 25 Šolcová O., Schneider P.: Multicomponent Counter-Current Gas Diffusion: Determination of Transport Parameters. Appl. Catal., A 244(1), 1-9 (2003).

O 26 Šolcová O., Šnajdaufová H., Schneider P.: Liquid-Expulsion Perm-Porometry (LEPP) for Characterization of Porous Solids. Micropor. Mesopor. Mat. 65(2-3), 209-217 (2003).

O 29 Šolcová O., Schneider P.: Axial Dispersion in Single Pellet-String Columns with Non-Porous Packing. Chem. Eng. Sci. 59(6), 1301-1307 (2004).

O 33 Šolcová O., Soukup K., Schneider P.: Axial Dispersion in Single Pellet-String Columns Packed with Unusually Shaped Porous Pellets. Chem. Eng. J. 110(1-3), 11-18 (2005).

O 34 Hejtmánek V., Schneider P., Soukup K., Šolcová O.: Comparison of Transport Characteristics and Textural Properties of Porous Material; the Role of Pore Sizes and Their Distributions. Stud. Surf. Sci. Catal. 160, 217-224 (2006).

O 36 Starý T., Šolcová O., Schneider P., Marek M.: Effective Diffusivities and Pore-Transport Characteristics of Washcoated Ceramic Monolith for Automotive Catalytic Converter. Chem. Eng. Sci. 61(18), 5934-5943 (2006).

O 37 Šolcová O., Hejtmánek V., Šnajdaufová H., Schneider P.: Liquid Expulsion Permporometry – a Tool for Obtaining Distribution of Flow Through Pores. Part. Part. Syst. Charact. 23(1), 40-47 (2006).

O 38 Šolcová O., Matějová L., Schneider P.: Pore-size Distributions from Nitrogen Adsorption Revisited: Models Comparison with Controlled-pore Glasses. Appl. Catal., A 313(2), 167-176 (2006).

O 39 Šolcová O., Soukup K., Schneider P.: Diffusion Coefficients and Other Transport Characteristics of Peculiarly Shaped Porous Materials in the Single Pellet-String Column. Micropor. Mesopor. Mat. 91(1-3), 100-106 (2006).

O 44 Matějová L., Schneider P., Šolcová O.: Standard (Master) Isotherms of Alumina, Magnesia, Titania and Controlled-Pore Glass. Micropor. Mesopor. Mat. 107(3), 227-232 (2008).

O 45 Schneider P., Hudec P., Šolcová O.: Pore-Volume and Surface Area in Microporous-Mesoporous Solids. Micropor. Mesopor. Mat. 115(3), 491-496 (2008).

O 46 Soukup K., Schneider P., Šolcová O.: Comparison of Wicke-Kallenbach and Graham's Diffusion Cells for Obtaining Transport Characteristics of Porous Solids. Chem. Eng. Sci. 63(4), 1003-1011 (2008).

O 47 Soukup K., Schneider P., Šolcová O.: Wicke-Kallenbach and Graham's Diffusion Cells; Limits of Application for Low Surface Area Porous Solids. Chem. Eng. Sci. 63(18), 4490-4493 (2008).

O 49 Kočí K., Obalová L., Matějová L., Plachá D., Lacný A., Jirkovský J., **Šolcová O.**: Effect of TiO2 Particle Size on the Photocatalytic Reduction of CO2. Appl. Catal., B 89(3-4), 494-502 (2009).

O 51 Šolcová O., Soukup K., Rogut J., Stanczyk K., Schneider P.: Gas Transport through Porous Strata from Underground Reaction Source; the Influence of the Gas Kind, Temperature and Transport-Pore Size. Fuel Process. Technol. 90(12), 1495-1501 (2009).

O 56 Kočí K., Matějů K., Obalová L., Krejčíková S., Lacný Z., Plachá D., Čapek L., Hospodková A., Šolcová O.: Effect of Silver Doping on the TiO2 for Photocatalytic Reduction of CO2. Appl. Catal., B 96(3-4), 239-244 (2010).

O 60 Soukup K., Petráš D., Klusoň P., Šolcová O.: Nanofiber Membranes—Evaluation of Gas Transport. Catal. Today 156(3-4), 316-321 (2010).

O 66 Šolcová O., Matějová L., Topka P., Musilová Z., Schneider P.: Comparison of Textural Information from Argon (87 K) and Nitrogen (77 K) Physisorption. J. Porous Mat. 18(5), 557-565(2011).

O 72 Krejčíková S., Matějová L., Kočí K., Obalová L., Matěj Z., Čapek L., Šolcová O.: Preparation and characterization of Ag-doped crystalline titania for photocatalysis applications. Appl. Catal. B: Environ. (2011), doi:10.1016/j.apcatb.2011.09.024

O 75 Šolcová O., Schneider P.: Experimental Determination of Transport Parameters. In: Gas Transport in Porous Media. (Ho, C.K. - Webb, S.W., Ed.), pp. 245-272, Springer, Dordrecht 2006.

O 76 Soukup K., Rogut J., Grabowski J., Wiatowski M., Ludwik-Pardala M., Schneider P., Šolcová O.: Porous Iron and Ferric Oxide Pellets for Hydrogen Storage: Texture and Transport Characteristics. In: Advances in Control, Chemical Engineering, Civil Engineering and Mechanical Engineering., pp. 99-103, WSEAS Press, Atény 2010.

9 References

[1] Wang Q., Jiang Z.Y, Wang Y.B., Chen D.M., Yang D., J. Nanopart. Res. 11, 375-384 (2009).

[2] Liu Y., Wang X.L., Yang F., Yang X.R., Micro. Meso. Mat. 114, 431-439 (2008).

[3] Ramakrishna S., Fujihara K., Lim W.-C., Ma Z.: An Introduction to Electrospinning and Nanofibers. World Scientific Publishing Ltd, Singapore, 2005.

[4] Sui R., Rizkalla A., Charpentier P.A.: Experimental study on the morphology and porosity of TiO2 aerogels synthesized in supercritical carbon dioxide. Microporous and Mesoporous Materials (2011), in press.

[5] Shimoyama Y., Ogata Y., Ishibashi R., Iwai Y., Chemical Engineering Research and Design 88(10), 1427-1431 (2010).

[6] Tursiloadi S., Yamanaka Y., Hirashima H., Journal of Sol-Gel Science and Technology 38, 5-12 (2006).

[7] Huang X.-J., Ge D., Xu Z.-K., Eur. Polymer. J. 43, 3710 (2007).

[8] Sakai S., Liu Y., Yamaguchi T., Watanabe R., Kawabe M., Kawakami K., Biores. Technol. 101, 7344 (2010).

[9] Wang Z.-G., Wan L.-S., Liu Z.-M., Huang X.-J., Xu Z.-K., J. Mol. Catal. B Enzym. 56, 189 (2009).

[10] Webb P.A., Orr C.: Analytical Methods in Fine Particle Technology. Micromeritics Instrument Corporation, Norcross, 1997.

[11] Barret E.P., Joyner L.G., Halenda P.B., J. Am. Chem. Soc. 73, 373 (1951).

[12] Halsey G., J. Chem. Phys. 16 (10), 931-937 (1948).

[13] Harkins W.B., Jura G., J. Am. Chem. Soc. 66 (8), 1366 (1944).

[14] deBoer J.B., Lippens B.C., Linsen B.G., Broekhoff J.C.P., Heuvel A.V.D., Osinga Th.J., J. Colloid Interface Sci. 21, 405 (1966).

[15] Yaws C.L. (Ed.): Chemical Properties Handbook, Mc-Graw-Hill, 1999.

[16] ASAP 2010 User's Manual, Micromeritics, USA, 1996.

[17] Broekhoff J.C., deBoer J.H., J. Catal. 9, 8 (1967).

[18] Broekhoff J.C., deBoer J.H., J. Catal. 9, 15 (1967).

[19] Broekhoff J.C., deBoer J.H., J. Catal. 10, 153 (1968).

[20] Broekhoff J.C., deBoer J.H., J Catal. 10, 368 (1968).

[21] Broekhoff J.C., deBoer J.H., J. Catal. 10, 377 (1968).

[22] Lecloux A., in: S. Modrý, M. Svatá (Eds.): Proc. Internat. Symp. RILEM/IUPAC, Part II, vol. IV, Academia Praha, pp. 427-432, 1978.

[23] Elmer T.H.: Porous and Reconstructed Glasses, Engineered Materials Handbook, vol. 4, Ceramic and Glasses, ASM International, MaterialsPark, Ohio, 1992.

[24] Brunauer S., Emmett P.H., Teller E., J. Am. Chem. Soc. 60, 309 (1938).
[25] Schneider P., Appl. Catal. A 129, 157 (1995).
[26] Gregg S.J., Sing K.S.W.: Adsorption, Surface Area and Porosity, second ed., Academic Press, London, 1982.
[27] Rouquerol J., Rouquerol F., Sing K.S.W.: Adsorption by Powders and Porous Solids, Academic Press, London, 1999.
[28] Jacobsen R.T., Penoncello S.G., Lemdmon E.W.: Thermodynamic Properties of Cryogenic Fluids, Kluwer, 1997.
[29] Sah A., Castricum H.L., Bliek A., Blank D.H.A., ten Elshof J.E., Journal of Membrane Science 243(1-2), 125-132 (2004).
[30] Chowdhury S.R., Schmuhl R., Keizer K., ten Elshof J.E., Blank D.H.A., Journal of Membrane Science 225(1-2), 177-186 (2003).
[31] Tsuru T., Hino T., Yoshioka T., Asaeda M., Journal of Membrane Science 186(2), 257-265 (2001).
[32] Nishiyama N., Saputra H., Park D.H., Egashira Y., Ueyama K., Journal of Membrane Science 218(1-2), 165-171 (2003).
[33] Solberg D., Wagberg L., Journal of Pulp and Paper Science 28(6), 183-188 (2002).
[34] Schneider P., Chemical Engineering Science 33, 1311-1319 (1978).
[35] Mann R., Thomson G., Chem. Eng. Sci., 42, 555-563 (1987).
[36] Sahimi M.: Flow and transport in porous media and fractured rock: from classical methods to modern approaches. VCH, Weinheim, 1995.
[37] Petropoulos J.H., Petrou J.K., Liapis A.I., Ind. Eng. Chem. Res. 30, 1281-1289 (1991).
[38] Schneider P., Gelbin D., Chem. Eng. Sci. 40,1093-1099 (1984).
[39] Fott P., Petrini G., Schneider P., Coll. Czech. Chem. Commun 48, 215-227 (1983).
[40] Mason E.A., Malinauskas A.P.: Gas Transport in Porous Media, The Dusty Gas Model. Elsevier, Amsterdam, 1983.
[41] Jackson R.: Transport in Porous Catalysts. Elsevier, Amsterdam, 1977.
[42] Novák M., Ehrhard K., Klusáček K., Schneider P., Chem. Eng. Sci. 43, 185-193 (1988).
[43] Mason E.A., Maulinauskas A.P., Evans J.W., J. Chem. Phys. 46, 3199-3217 (1967).
[44] Rothfeld L.B., A.I.Ch.E.J. 9, 19-24 (1963).
[45] Wicke E., Kallenbach R., Kolloid Zeitschrift 97, 135-151 (1941).
[46] Dogu G., Smith J.M., A.I.Ch.E. J. 21, 58-61 (1975).
[47] Haynes H.W., Canadian Journal of Chemical Engineering 56, 582-587 (1978).
[48] Krishna R., Industrial & Engineering Chemistry Fundamentals 16, 228-232 (1977).
[49] Krishna R., Chemical Engineering Journal 35, 75-81 (1987).
[50] Do H.D., Do, D.D., Chemical Engineering Science 53, 1239-1252 (1998).
[51] Krishna R., Wesselingh J.A., Chemical Engineering Science 52, 861-911 (1997).
[52] Kapteijn F., Moulijn J.A., Krishna R., Chemical Engineering Science 55, 2923-2930 (2000).
[53] Banat F.A., Al-Rub F.A., Shannag M., Heat Mass Transfer 35(5), 423-431 (1999).
[54] Tuchlenski A., Uchytil P., Seidel-Morgenstern A., Journal of Membrane Science 140(2), 165-184 (1998).
[55] Valuš J., Schneider P., Appl. Catal. 1, 355-366 (1981).
[56] Valuš J., Schneider P., Appl. Catal. 16, 329-341 (1985).
[57] Dullien F.A.L.: Porous Media– Fluid Transport and Pore Structure., Academic Press, New York, 1979.
[58] Sincovec R.R., Madsen N.K., ACM Trans. Math. Software 1, 261 (1975).
[59] Asaeda M., Watanabe J., Kitamoto M., J. Chem. Eng. Japan 14, 129 (1981).

[60] Keil F.: Diffusion und Chemische Reaktionen in der Gas/Feststoff-Katalyse. Springer Press, Berlin, 1999.
[61] Haugaard J., Livbjerg H., Chemical Engineering Science 53 (16), 2941-2948 (1998).
[62] Čapek P., Seidel-Morgenstern A., Applied Catalysis, A General 211, 227 (2001).
[63] Hou K., Fowles M., Hughes R., Chemical Engineering Research & Design 77 (A1), 55-61 (1999).
[64] Szymczyk A., Labbez C., Fievet P., Vidonne A., Foissy A., Pagetti J., Advances in Colloid and Interface Science 103 (1), 77-94 (2003).
[65] Schneider P., Smith J.M., AIChE Journal 14(5), 762-771 (1968).
[66] Haynes H.W., Catalysis Review-Science and Engineering 30(4), 563-627 (1988).
[67] Scott D.S., Lee W., Papa J., Chemical Engineering Science 29(11), 2155-2167 (1974).
[68] Li T., Zhu Y., Li S., Zhu J., Zhu B., Journal of East China University of Science and Technology 26(3), 256-259 (2000).
[69] Sun W., Costa C.A.V., Rodrigues A.E., Industrial and Engineering Chemistry Research 33(5), 1380-1390 (1994).
[70] Li J., Pan Y., Chen M., Zhu B., Fuel Science and Technology International 13(7), 857-879 (1995).
[71] Colaris A.H.J., Hoebink J.H.B.J., de Croon M.H.J.M., Schoulen J.C., AIChE Journal 48(11), 2587-2596 (2002).
[72] Yu G., Yu J., Yu Z., Chemical Engineering Journal 78(2-3), 141-146 (2000).
[73] Li P., Xiu G., Rodrigues A.E., Chemical Engineering Science 59, 3091-3103 (2004).
[74] Hong L., Felinger A., Kaczmarski K., Guiochon G., Chemical Engineering Science 59, 3399-3412 (2004).
[75] Schneider P., Smith J. M., AICHE J. 14, 886-895 (1968).
[76] Kubín M., Collection of the Czechoslovak Chemical Communications 30, 1104-1118 (1965).
[77] Kučera E., Journal of Chromatography 19, 237-248 (1965).
[78] Fahim M.A., Wakao N., Chem. Eng. J. 25, 1-8 (1982).
[79] Wakao N., Kaguei S., Smith J.M., J. Chem. Eng. Japan 12, 481-485 (1979).
[80] Schneider P., Chem. Eng. Sci. 39, 927-929 (1984).
[81] Edwards M.F., Richardson J.F., Canadian Journal of Chemical Engineering 48, 466-467 (1970).
[82] Beale E.M.L., J. Roy. Stat. Soc. B22, 41, (1960).
[83] Cybulski A., Moujin J.A.: The present and the future of structured catalysts. In: Cybulski A., Moujin J.A. (Eds.), Structured Catalysts and Reactors. Marcel Dekker, New York, pp. 1-14, 1998.
[84] Kašpar J. et al., Catalysis Today 77, 419-449 (2003).
[85] Gulati S.T.: Ceramic catalyst supports for gasoline fuel. In: Cybulski A., Moujin J.A. (Eds.), Structured Catalysts and Reactors. Marcel Dekker, New York, pp. 15-58, 1998.
[86] Heck R.M., Farrauto R.J.: Catalytic Air Pollution Control: Commercial Technology. Van Nostrand Reinhold, New York, pp. 11-26, 1995.
[87] Twigg M.V., Wilkins A.J.J.: Autocatalysts - past, present and future. In: Cybulski A., Moujin J.A. (Eds.), Structured Catalysts and Reactors. Marcel Dekker, New York, pp. 91-120, 1998.
[88] Kočí P. et al., Industrial and Engineering Chemistry Research 43, 4503-4510, (2004).

[89] West D.H. et al., Catalysis Today 88, 3-16, (2003).
[90] Mukadi L.S., Hayes R.E., Computers and Chemical Engineering 26, 439-455, (2002).
[91] Leung D. et al., Canadian Journal of Chemical Engineering 74, 94-103, (1996).
[92] Ramathan K. et al., Chemical Engineering Science 58, 1381-1405, (2003).
[93] Friedmann S.J., Upadhye R., Kong F.M., Energy Procedia 1, 4551-4557 (2009).
[94] Kreinin E.B., Coal. Chem. Ind. 6, 61-63 (1993).
[95] Yang L., Liang J., Yu L., Energy 28, 1445-1460 (2003).
[96] Yang L., Zhang X., Liu S., Yu L., Zhang W., Int. J. Hydrogen Energy 33, 1275-1275 (2008).
[97] Huang X.J., Ge D., Xu Z.K., Eur. Polym. J. 43, 3710 (2007).
[98] Ramakrishna S., Fujihara K.: An Introduction to Electrospinning and Nanofibers, World Scientific Publishing Ltd, Singapore, 2005.
[99] Greiner A., Wendorff J.H., Chem. Int. Ed. 46, 5670 (2007).
[100] Subbiah T., Bhat G.S., Tock R.W., Parameswaran S., Ramkumar S.S., J. Appl. Polym. Sci. 96, 557 (2005).
[101] Park S., Park K., Yoon H., Son J., Min T., Kim G., Polym. Int. 56, (2007).
[102] Stasiak M., Röben C., Rosenberger N., Schleth F., Studer A., Greiner A., Wendorff J.H., Polymer 48, 5208 (2007).
[103] Wan L.S., Ke B.B., Xu Z.K., Enzyme Microb. Technol. 42, 332 (2008).
[104] Peña J. A., Lorente E., Romero E., Herguido J., Catal. Today 116, 439-444 (2006).
[105] Svoboda K., Slowinski G., Rogut J., Baxter D., Energy Convers. Manag. 48, 3063-3073 (2007).
[106] Lorente E., Peña J.A., Herguido J., Int. J. Hydrogen Energy 33, 615-626 (2008).
[107] Maira A.J., Yeung K.L., Soria J., Coronado J.M., Belver C., Lee C.Y., Augugliaro V., Appl. Catal. B 29, 327 (2001).
[108] Krysa J., Waldner G., Mestankova H., Appl. Catal. B 64, 290 (2006).
[109] Machalicky O., Lichy L., Badura J., J. Photochem. Photobiol. A 180, 28 (2006).
[110] Kitiyanan A., Yoshikawa S., Materials Letters 59, 4038 (2005).
[111] Dagaonkar M.V., Heeres H.J., Beenackers A.A.C.M., Pangarkar V.G., Chem. Eng. J. 9, 151 (2003).
[112] Sreethawong T., Suzuki Y., Yoshikawa S., J. Solid State Chem. 178, 329 (2005).
[113] Kitano M., Matsuoka M., Ueshima M., Anpo M., Appl. Catal. A 325, 1 (2007).
[114] Thompson T.L., Yates J.T., Topics in Catalysis 35, 197 (2005).
[115] Sulakova R., Hrdina R., G.M.B., Dyes and Pigments 73, 19 (2007).